European Journal of Medicinal Chemistry 162 (2019) 631–649

Contents lists available at ScienceDirect

European Journal of Medicinal Chemistry

journal homepage: http://www.elsevier.com/locate/ejmech

Research paper

Structure-based exploration and pharmacological evaluation of *N*-substituted piperidin-4-yl-methanamine CXCR4 chemokine receptor antagonists

I. Adlere [a, 1], S. Sun [b, 1], A. Zarca [b, 1], L. Roumen [b], M. Gozelle [b, c], C. Perpiñá Viciano [d, e], B. Caspar [f], M. Arimont [b], J.P. Bebelman [b], S.J. Briddon [f], C. Hoffmann [d, e], S.J. Hill [f], M.J. Smit [b], H.F. Vischer [b], M. Wijtmans [b], C. de Graaf [b], I.J.P. de Esch [a, b], R. Leurs [a, b, *]

[a] Griffin Discoveries BV, Amsterdam, the Netherlands
[b] Division of Medicinal Chemistry, Amsterdam Institute for Molecules, Medicines and Systems, Faculty of Science, Vrije Universiteit Amsterdam, De Boelelaan 1108, 1081 HZ Amsterdam, the Netherlands
[c] Department of Pharmaceutical Chemistry, Faculty of Pharmacy, Gazi University, 06560, Ankara, Turkey
[d] Institute for Molecular Cell Biology, CMB-Center for Molecular Biomedicine, University Hospital Jena, Friedrich-Schiller University Jena, Hans-Knöll-Strasse 2, 07745, Jena, Germany
[e] Institute of Pharmacology and Toxicology, University of Würzburg, Versbacher Str. 9, 97078, Würzburg, Germany
[f] Division of Pharmacology, Physiology and Neuroscience and Centre of Membrane Proteins and Receptors (COMPARE), School of Life Sciences, University of Nottingham, Nottingham, NG7 2UH, UK

ARTICLE INFO

Article history:
Received 12 September 2018
Received in revised form
23 October 2018
Accepted 27 October 2018
Available online 30 October 2018

Keywords:
G protein-coupled receptors
CXCR4 chemokine receptor
Antagonists
Structure-based fragment virtual screening
Structure-activity relationship
3D-QSAR

ABSTRACT

Using the available structural information of the chemokine receptor CXCR4, we present hit finding and hit exploration studies that make use of virtual fragment screening, design, synthesis and structure-activity relationship (SAR) studies. Fragment **2** was identified as virtual screening hit and used as a starting point for the exploration of 31 N-substituted piperidin-4-yl-methanamine derivatives to investigate and improve the interactions with the CXCR4 binding site. Additionally, subtle structural ligand changes lead to distinct interactions with CXCR4 resulting in a full to partial displacement of CXCL12 binding and competitive and/or non-competitive antagonism. Three-dimensional quantitative structure-activity relationship (3D-QSAR) and binding model studies were used to identify important hydrophobic interactions that determine binding affinity and indicate key ligand-receptor interactions.
© 2018 Elsevier Masson SAS. All rights reserved.

1. Introduction

Chemokines and G protein-coupled chemokine receptors (GPCRs) play an important role in the immune defense system by controlling the migration, activation, differentiation, and survival of leukocytes [1]. Endogeneous chemokine proteins stabilize their cognate chemokine receptors in an active conformation that facilitates intracellular signal transduction by interactions with G proteins and/or arrestins [1,2]. Because of their crucial role in the migration of immune cells, chemokine receptors are promising drug targets for various immune-related diseases, including chronic obstructive pulmonary disease, multiple sclerosis, rheumatoid arthritis, HIV-1 infection and cancer [3,4]. Molecular pharmacology, medicinal chemistry and molecular modelling studies

Abbreviations: GPCR, G protein-coupled receptor; CXCR4, C-X-C chemokine receptor type 4; SAR, structure-activity relationship; BRET, bioluminescence resonance energy transfer; TMD, transmembrane domain; SDF-1, stromal derived factor-1; SBVS, structure-based virtual screening; FBLD, fragment-based ligand design; IFP, interactions fingerprint; QSAR, quantitative structure-activity relationship; H-bond, hydrogen bond; MD, molecular dynamics; LE, ligand efficiency; LLE, ligand-lipophilicity efficiency; FRET, fluorescence resonance energy transfer; IP, inositol phosphate.

* Corresponding author. Division of Medicinal Chemistry, Amsterdam Institute for Molecules, Medicines and Systems, Faculty of Science, Vrije Universiteit Amsterdam, De Boelelaan 1108, 1081 HZ Amsterdam, the Netherlands.
E-mail address: r.leurs@vu.nl (R. Leurs).

[1] Author Contributions: Ilze Adlere, Shan-Liang Sun and Aurélien Zarca contributed equally to this work.

https://doi.org/10.1016/j.ejmech.2018.10.060
0223-5234/© 2018 Elsevier Masson SAS. All rights reserved.

have provided insights into molecular determinants of chemokine receptor modulation by proteins, peptides, and small-molecule ligands [1,5]. In the past few years, the first high-resolution crystal structures of chemokine receptors have been solved and these have given detailed structural information on the interaction of chemokine receptors and their ligands [6]. The crystal structures of vMIP bound CXCR4 [7], CCL5 bound CCR5 [8], and CX3CL1 bound US28 [9] complexes show how chemokine ligands bind the N-terminal and extracellular loop regions of the receptor with their relatively conserved C-terminal domains and target the orthosteric seven-transmembrane helical domain (TMD) with their variable N-terminal regions [5]. Moreover, CCR2, CCR5 and CXCR4 crystal structures show how small-molecule drug-like ligands (BMS-681, maraviroc, IT1t, Fig. 1) and medium sized peptidomimetic (CVX15) target the TMD binding site ("ancestral" orthosteric binding site [10]) and block the binding of the chemokine N-terminus [6,11,12]. Recent CCR2 and CCR9 crystal structures reveal that chemokine receptors may also contain a conserved intracellular allosteric binding site overlapping with the G protein coupling site that can be targeted by small drug-like ligands (CCR2-RA-[*R*], Vercirnon) [12–15]. Despite these breakthroughs in the elucidation of crystal structures of chemokine receptors, the computational prediction of receptor-ligand interactions to guide structure-based ligand discovery is still facing several challenges. The large, open and solvent accessible orthosteric TMD binding sites of chemokine receptors are challenging targets for structure-based virtual ligand screening [5] compared to the more druggable, occluded binding sites of e.g. aminergic GPCRs [16,17]. To effectively interact with these binding sites, most chemokine receptor ligands are relatively large and/or hydrophobic, and contain multiple cationic centers to interact with conserved negatively charged residues in chemokine receptors.

Hallmark chemokine receptor CXCR4 is activated by the endogeneous chemokine CXCL12 (also known as stromal cell-derived factor-1, SDF-1α) and targeted by the antagonist plerixafor/AMD3100 (Fig. 1), the first approved drug acting on chemokine receptors and used for stem cell mobilization [18]. The CXCR4 receptor was the first chemokine receptor to be crystallized with small-molecule, peptide, and chemokine ligands and provides an ideal system to investigate the possibilities and limitations of structure-based ligand design [19,20]. Chemokine receptor modelling studies, including the community-wide GPCR DOCK 2010 assessment to predict the three-dimensional coordinates of the IT1t and CVX15 bound CXCR4 crystal structures, have identified several pitfalls associated with matching the interaction properties of chemokine receptor binding sites and small-molecule ligands [21]. Firstly, the possibilities to translate binding mode hypotheses between chemokine receptors and/or ligand chemotypes is limited by: i) the symmetric distribution of anionic residues in the receptor (e.g. $D^{2.63}$, $D^{4.60}$, $D^{6.58}$, $E^{7.39}$ in CXCR4) and complementary cationic centers in known tool compounds (e.g. AMD3100, IT1t), ii) the existence of multiple orthosteric and allosteric small-molecule binding pockets, and iii) the ligand dependent effects of receptor mutation studies [5]. Secondly, the structure-based identification and optimization of chemokine receptor ligands is complicated by conformational sampling of larger, flexible ligands and receptor binding sites as well as by defining effective scoring methods for the prioritization of potential ligands based on their predicted interactions with solvent accessible receptor binding sites [5]. Several potent small-molecule ligand classes, such as the ones exemplified by IT1t and AMD3100, have been identified for CXCR4 (Fig. 1) [18,22–29] Virtual screening campaigns to discover novel CXCR4 ligands mostly yielded high micromolar binding affinities (IC_{50}, K_i) [30,31] or no measurable binding affinity in radiolabeled chemokine displacement studies [32,33] and, considering the low ligand efficiency (delta free energy of binding divided by the number of heavy atoms [34]) of these hits, the potential for successful optimization was not evident. Considering the low LE values, it is no surprise that fragment-based approaches for peptidergic GPCRs such as chemokine receptors have so far been relatively scarce [5], especially when compared to other GPCRs like adenosine and aminergic GPCRs, for which *in silico* fragment screening and hit exploration was very successful [35,36]. Starting point for our studies was a virtual screening hit that contains an *N*-substituted piperidin-4-yl-methanamine core. Several piperidine-containing CXCR4 ligand classes have been reported [30,31], including AMD3100 derivatives [37], dual CCR5/CXCR4 inhibitors [38], benzenesulfonamides [39] and *N*-substituted benzimidazoles [40]. Here we used a fragment-based approach that makes use of the CXCR4 structural information and molecular modelling studies to complement the structure-activity relationship (SAR) studies during hit exploration.

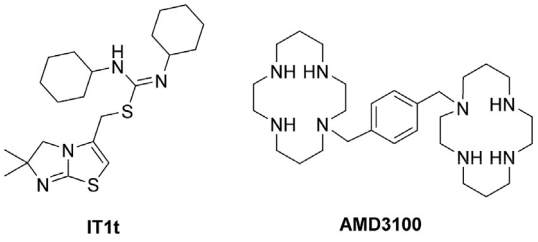


Fig. 1. Selected CXCR4 reference antagonists.

2. Results and discussion

2.1. Structure-based virtual screening

We designed a structure-based virtual screening workflow focusing on the identification of small, fragment-like molecules [41] and customized this to experimentally supported [5] CXCR4 ligand interaction features (HB and ionic interactions with residues $D97^{2.63}$ and $E288^{7.39}$) (Fig. 2A). In the first step, a focused chemical library was prepared containing fragment-like molecules (number of heavy atoms ≤ 22, logP < 3, number of H-bond donors ≤ 3, number of H-bond acceptors ≤ 3, number of rotatable bonds ≤ 5, number of rings ≥ 1) with two basic centers, consistent with the conserved cationic pharmacophore features of IT1t and AMD3100 (Fig. 1) and complementary to the negatively charged residues $D97^{2.63}$, $D171^{4.60}$, $D262^{6.58}$, $E288^{7.39}$ that have been shown to play a role in small-molecule ligand binding to CXCR4 [5]. This focused virtual library of 52.500 fragment-like molecules with two cationic centers was docked in the CXCR4 crystal structure (PDB ID: 3ODU) [6] using GOLD [42] and PLANTS [43] docking algorithms. Molecules that were able to simultaneously form H-bond and ionic interactions with $D97^{2.63}$ and $E288^{7.39}$ were ranked according to their GOLD (503 compounds) and PLANTS (1414 compounds) docking scores, as well as their structural Interaction FingerPrint (IFP) [44] compared to the co-crystallized IT1t reference (Fig. 2B). The docking poses of the top 200 ranked molecules were visually inspected, and molecules with polar groups docked in the previously identified hydrophobic hot spot between $W94^{2.60}$ and $Y116^{3.33}$ were discarded [45]. A structural novelty filter (ECFP-4< 0.4 [46] as compared with any known CXCR4 ligands) resulted in a final selection of 34 fragment-like compounds, of which 23 commercially available compounds (specified in Fig. S1) were purchased and validated in ^{125}I-CXCL12 binding studies.

Tested at 63 μM, four hits (**1**–**4**) showed more than 50% inhibition of ^{125}I-CXCL12 binding to HEK293T cell membranes transiently overexpressing human CXCR4 (Fig. 2C) and these were selected for further evaluation. Fragments **2** and **3** share the same benzylpiperidin-4-yl-methanamine scaffold and fragment **3** was therefore discarded from further validation. Fragment hit **4** holds a chiral

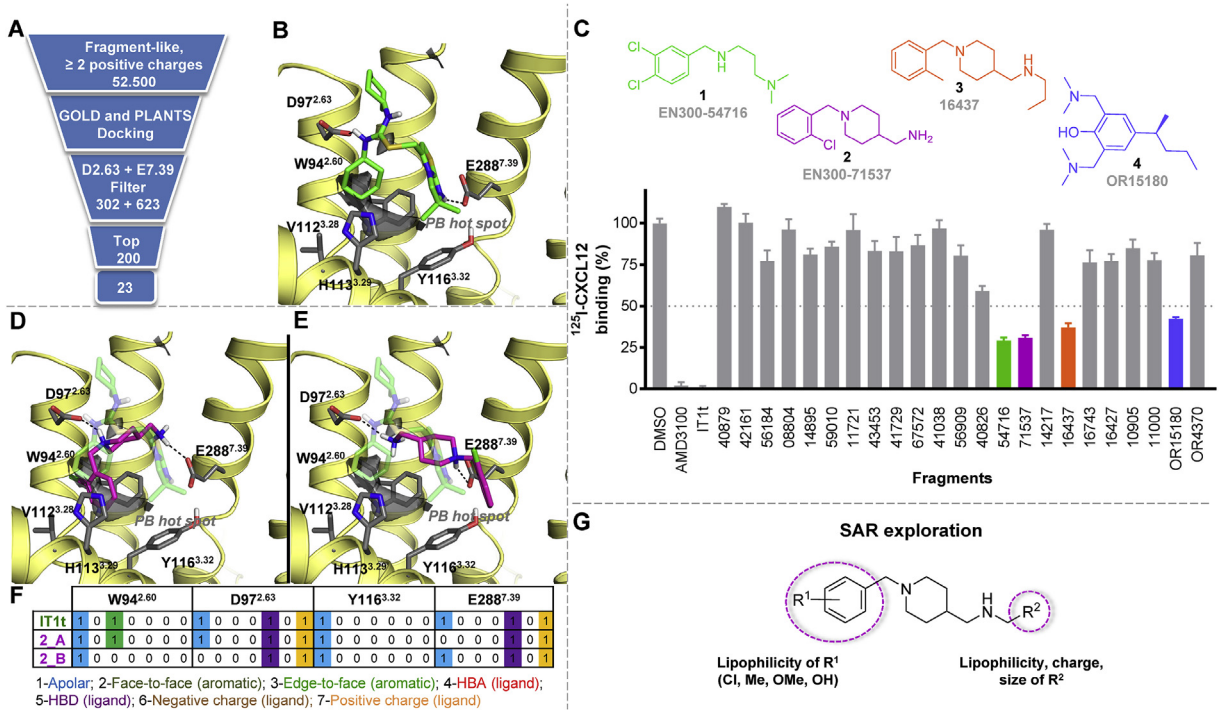


Fig. 2. Overview of the structure-based (SB) ligand virtual screen and design (A–G).
(A) Overview of the different steps in the SB virtual screening work flow. (B) Compound IT1t (green stick) binding to CXCR4 (yellow cartoon, PDB ID: 3ODU [6]). Key residues are shown as grey sticks and protein-based (PB) hydrophobic hot spots are shown in transparent grey surface. (C) Single concentration (63 μM) binding studies of 23 commercially available SBVS hit analogues and the structures of four hits showing more than 50% inhibition of ^{125}I-CXCL12 binding to human CXCR4. (D-E) Two alternative binding modes of **2** (magenta stick) binding to CXCR4. IT1t is shown in transparency as a reference. Key residues are shown in grey stick and PB hot spots are shown in transparent grey surface. (F) Comparative structural interaction fingerprint (IFP) [44] analysis of binding modes of IT1t and **2**. The structural receptor–ligand interaction patterns are described by IFP bit strings encoding different interaction types between the ligand and receptor CXCR4 amino acid residues. (G) Schematic illustration of SAR exploration of N-substituted piperidin-4-yl-methanamines.

center and can potentially form a reactive quinone moiety and further growing from this fragment was therefore deprioritized. The two remaining hits **1** and **2** were subsequently tested for concentration-dependent inhibition of ^{125}I-CXCL12 binding to hCXCR4 (IC_{50}, Table 1), resulting in a better pIC_{50} value (5.0) for fragment **2** than for **1**.

Docking studies of **2** into the X-ray structure of hCXCR4 (PDB ID: 3ODU [6]) suggest two alternative binding modes (Fig. 2D and E), which both include ionic and H-bond interactions with D97$^{2.63}$ and E288$^{7.39}$, consistent with the binding mode of IT1t in the CXCR4 crystal structure (Fig. 2B) [6]. In binding mode 1, compound **2** accommodates its chlorinated phenyl group in the hydrophobic hot spot of CXCR4 between TM helices 1–3 and 7 [5,45] (Fig. 2D), whereas in binding mode 2 the chlorinated phenyl group is directed towards the major binding pocket of CXCR4 between TM helices 3–7 (Fig. 2E). Structural Interaction FingerPrint (IFP) analysis [47] of IT1t and these two poses of compound **2** (Fig. 2F) shows shared interactions with key residues (W94$^{2.60}$, D97$^{2.63}$, Y116$^{3.32}$ and E288$^{7.39}$). The two alternative binding mode hypotheses and structural analyses were used to guide fragment growing studies to explore structure-activity relationships and improve the virtual screening hit **2.** The ensuing design strategy involved substitutions of varying chemical nature on both amine moieties of the scaffold (Fig. 2G).

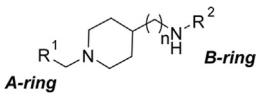
2.2. Chemistry

The synthesis of the compounds based on **2** is outlined in Scheme 1. Compounds **6a,b,d-l** were prepared in a direct one-pot reductive amination of benzaldehydes and commercially available 4-(Boc-aminomethyl)piperidine **5a** or 4-(Boc-aminoethyl) piperidine **5b** (in case of **6f**) in the presence of $NaBH(OAc)_3$. Compound **6c** was obtained by alkylation of amine **5a** with 1-(chloromethyl)-2-methylbenzene and K_2CO_3. Deprotection of **6a-l** with HCl in dioxane, followed by a basic workup (except for compounds **7g** and **7h,** which were isolated as hydrochloride salts) provided key building blocks **2** and **7b-l**. The final compound series **8**–**32** was obtained in a two-step reductive amination of benzaldehydes and **2, 7d,g-l** *via* imine formation (followed by ^{1}H NMR spectroscopy on isolated aliquots), following by reduction with $NaBH_4$ in MeOH. Compounds **20, 21** and **29** retained traces of the benzylic alcohol (formed from the starting benzaldehyde during $NaBH_4$ treatment) even after acid/base workup and crystallization as fumarate salts proved efficient to remove these impurities.

2.3. Structure-activity relationship

We synthesised and evaluated a variety of analogues of hit fragment **2**. As depicted in Table 1, the left-hand ring of the scaffold bearing substituent R^1 and the right-hand ring with R^2 substitution are assigned as the A-ring and B-ring, respectively. To evaluate the binding affinity, displacement assays were performed in which ^{125}I-CXCL12 binding to human CXCR4 was displaced by the ligands at multiple concentrations (Table 1). As partial or no displacement of CXCL12 binding by small-molecule CXCR4-binding ligands is a known phenomenon [38], we also monitored the extent of displacement at 100 μM concentration of a ligand (Table 1). To assess the relative contributions of the different chemical modifications to CXCR4 binding affinity, we monitored the ligand efficiency (LE) and ligand-lipophilic efficiency (LLE) metrices (Table 1) [48]. We first explored a small series of analogues in which the 2-

Table 1
Binding affinity, level of inhibition of ^{125}I-CXCL12 binding and efficiency metrics for SBVS fragment hits and improved ligands.



2, **7-32**, n=1; **7f**, n=2

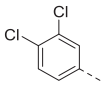
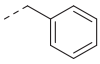
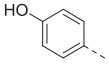
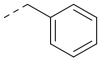
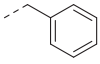
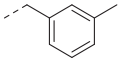
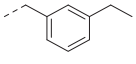
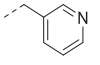
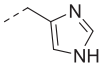
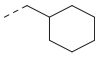
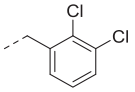
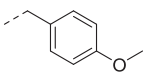
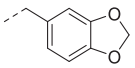
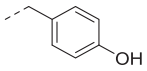
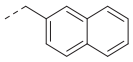
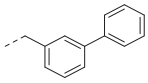
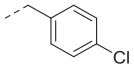
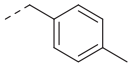
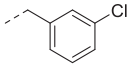
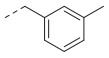
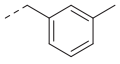
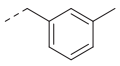
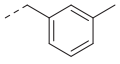
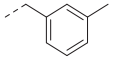
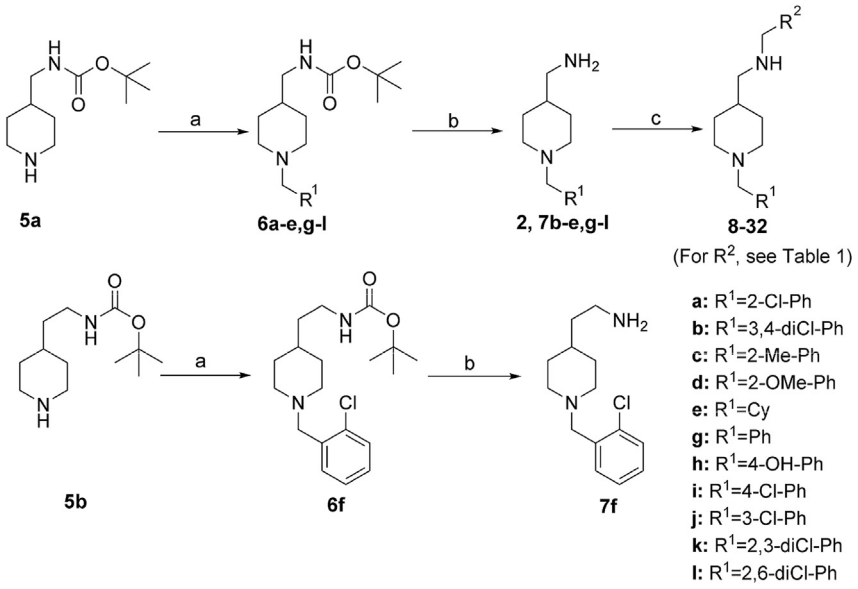
Compound	R^1 (A-ring)	R^2 (B-ring)	pIC_{50}[a]	^{125}I-CXCL12 displacement, %[b]	clogP	LE[c]	LLE[d]
CXCL12	–	–	9.3 ± 0.1	97 ± 0	–	–	–
AMD3100	–	–	6.7 ± 0.1	98 ± 3[e]	−0.25	0.25	6.78
IT1t	–	–	8.0 ± 0.0	100 ± 2	5.39	0.42	2.61
1	–	–	<5[e]	70 ± 3[e]	3.48	-[i]	-[i]
2		H	5.0 ± 0.0[e]	69 ± 2[e]	2.51	0.43	2.49
7b		H	<5	67 ± 6[f]	3.11	-[i]	-[i]
7c		H	<5	81 ± 4[f]	2.25	-[i]	-[i]
7d		H	<5	67 ± 4[f]	1.72	-[i]	-[i]
7e		H	<5	59 ± 3[f]	2.49	-[i]	-[i]
7f		H	<5	56 ± 6[f]	3.04	-[i]	-[i]
8			5.0 ± 0.1	72 ± 2	3.98	0.31	1.02
9			<5	65 ± 2[f]	3.31	-[i]	-[i]
10			5.6 ± 0.1	85 ± 1	3.89	0.32	1.74
11			6.1 ± 0.1	84 ± 3	4.39	0.33	1.67
12			6.1 ± 0.0	81 ± 1	4.92	0.32	1.14
13			6.5 ± 0.1[g]	87 ± 4	4.69	0.39	1.81
14			5.7 ± 0.2	89 ± 1	3.19	0.34	2.50
15			6.0 ± 0.1	96 ± 1	2.52	0.38	3.53
16			5.5 ± 0.1	77 ± 4	5.31	0.33	0.21
17			5.6 ± 0.3	13 ± 11	5.99	0.31	−0.40
18			5.9 ± 0.1	88 ± 2	4.61	0.32	1.29
19			6.6 ± 0.2	72 ± 3	4.65	0.35	1.97

Table 1 (*continued*)

Compound	R^1 (A-ring)	R^2 (B-ring)	pIC_{50}[a]	^{125}I-CXCL12 displacement, %[b]	clogP	LE[c]	LLE[d]
20			6.5 ± 0.2	98 ± 1	4.02	0.37	2.46
21[h]			6.3 ± 0.1	78 ± 1	5.86	0.32	0.40
22[h]			6.3 ± 0.0	98 ± 1	6.58	0.30	−0.27
23			6.2 ± 0.2	80 ± 4	5.40	0.35	0.81
24			6.0 ± 0.2	62 ± 1	5.19	0.34	0.82
25			6.7 ± 0.2	80 ± 4	5.40	0.38	1.31
26			6.6 ± 0.1	72 ± 5	5.14	0.38	1.50
27[h]			6.5 ± 0.1	65 ± 7	5.40	0.37	1.07
28			6.8 ± 0.1	63 ± 1	5.19	0.39	1.59
29			5.6 ± 0.1	86 ± 2	5.19	0.32	0.38
30			5.0 ± 0.1	86 ± 1	5.19	0.28	−0.19
31			6.1 ± 0.1	74 ± 2	5.78	0.33	0.28
32			6.6 ± 0.1	60 ± 3	5.90	0.36	0.67

[a] Measured as competition of ^{125}I-CXCL12 (50 pM) binding to hCXCR4 expressed in membranes of transiently transfected HEK293T cells. pIC_{50} values are means ± SEM (N = 3 with each experiment performed in triplicate).
[b] Percentage displacement of ^{125}I-CXCL12 (50 pM) in a presence of the ligand (100 μM) relative to IT1t (100 μM, 100%).
[c] Ligand efficiency LE = ΔG/HA = (− RT ln(IC_{50}))/HA, where R = 8.31447215 J/(K mol), T = 298.15 K, 1 kcal = 4184 J, HA = number of non-hydrogen atoms in molecule.
[d] Ligand-lipophilicity efficiency LLE = pIC_{50} − *c*logP, where *c*logP is calculated logP value of a compound and logP is the logarithm of the partition coefficient of the compound between n-octanol and water log($c_{octanol}/c_{water}$) [51].
[e] Measured as competition of ^{125}I-CXCL12 (40 pM) binding to hCXCR4 expressed in membranes of transiently transfected HEK293T cells. pIC_{50} values are means ± SEM (N = 3 with each experiment performed in triplicate). Percentage displacement calculated in a presence of the ligand (63 μM) relative to IT1t (63 μM, 100%).
[f] Full inhibition could not be achieved due to pIC_{50} < 5. The shown value is the percentage of inhibition detected at 100 μM.
[g] pIC_{50} value is mean ± SEM (N = 9 with each experiment performed in triplicate).
[h] Isolated and tested as fumarate salts.
[i] pIC_{50} value too low for accurate LE and LLE determination.

chlorophenyl moiety of **2** was varied (**7b-e**) to evaluate the effect of the substituent R^1. Comparing the SBVS hit **2** (pIC_{50} = 5.0) and its derivatives **7b-e** (pIC_{50} < 5), the *o*-chlorophenyl moiety shows the best results. Elongating the chain between the piperidine and the NH_2 group (**7f**) did not improve binding affinity. Considering ligand binding mode variability associated with the symmetric di-cationic pharmacophore [49] and chemical elaborations [50] of the central scaffold, we continued to probe the A-ring while appending several simple benzyl-type B-rings (**8**–**13**). Compounds **8** and **9** failed to show good affinity ($pIC_{50} \leq 5$), indicating the possible requirement for a lipophilic substitution on the A-ring. The *o*-methoxy analogue **10** (pIC_{50} = 5.6) gave a modest increase in affinity with respect to **8**, which could be further enhanced by a *m*-methyl or *m*-ethyl substituent on the B-ring (**11, 12**). However, as observed in the analogues without B-ring, the affinity of *o*-chlorophenyl analogue **13** (pIC_{50} = 6.6) was superior as it was 10-fold higher than that for *o*-methoxy substituted compound **10**, indicating a key overall contribution of the *o*-chlorophenyl substituent to the binding affinity. Compound **13** showed full displacement of ^{125}I-CXCL12 (Table 1, Fig. 3). Further exploration kept the *o*-chlorophenyl group



Scheme 1. Synthesis of CXCR4 ligands. Reagents and conditions: (a) $NaBH(OAc)_3$, DCE, R^1CHO (2-Cl-C_6H_4-CHO for **6f**), rt, 17 h–6 d, 33–98%; for **6c**: 1-(chloromethyl)-2-methylbenzene, K_2CO_3, EtOH, reflux, 3 h, 80%; (b) (i) 4 M HCl/dioxane, rt, 1–3 h; (ii) basic extraction, 58–99% (**7g** and **7h** isolated as dihydrochloride salts); (c) (i) R^2CHO, anhydrous Na_2SO_4, when using **7g** and **7h**: TEA, DCM, rt, 24 h–5 d; (ii) $NaBH_4$, MeOH, rt, 3–30 min, 46–96%; for **21, 22** and **27** (iii) fumaric acid, 2-PrOH, rt, 2–24 h, 38–52% as fumarate salt.

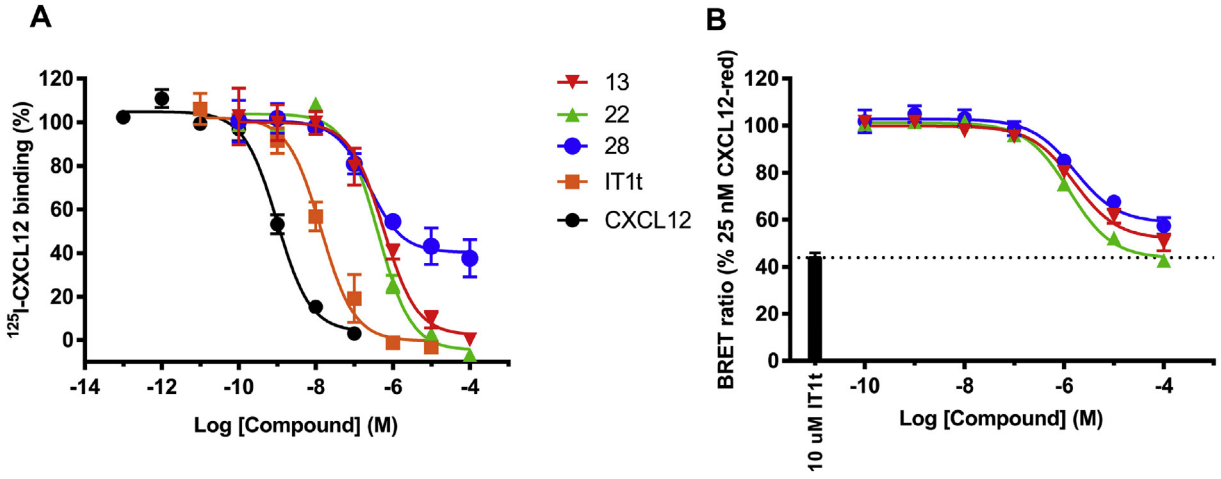


Fig. 3. (A) Inhibition of ^{125}I-CXCL12 binding to hCXCR4 expressed in HEK293T membranes by compounds **13**, **22** and **28**, and reference ligands IT1t and CXCL12. Representative curves are shown. Experiments were performed N ≥ 3 with each experiment performed in triplicate and mean values ± SEM are shown in Table 1 (B) The concentration-response curves for displacement of CXCL12-red binding to NLuc-tagged CXCR4 by selected ligands **13**, **22** and **28**. Curves are normalized to buffer (0%) and IT1t (100%). Experiments were performed N = 3 with each experiment performed in triplicate and mean values ± SEM are shown in Table S1. (For interpretation of the references to colour in this figure legend, the reader is referred to the Web version of this article.)

in place and was dedicated to exploring the preferred nature and substitutions of the B-ring. Replacing the phenyl B-ring in **13** with polar rings such as pyridine (**14**) or imidazole (**15**) resulted in reduced affinity ($pIC_{50} = 5.7$ and 6.0, respectively). Yet, both compounds displayed relatively high (89 and 96%) displacement of ^{125}I-CXCL12. The introduction of a cyclohexyl ring (**16,** $pIC_{50} = 5.5$) resulted in 12-fold decrease in affinity compared to **13**. A 2,3-dichlorophenyl substituent (**17**) displayed lower affinity ($pIC_{50} = 5.6$) and a remarkable loss of maximal displacement (13%) of ^{125}I-CXCL12 binding to hCXCR4. Derivatives with oxygen-based groups such as *p*-methoxy, *m,p*-methylenedioxy or *p*-hydroxy (**18**–**20**) showed moderate affinity and displacement, presenting no improvement with respect to **13**. Interestingly, the results for **20** ($pIC_{50} = 6.5$ and 98% of ^{125}I-CXCL12 displacement) contrast sharply to those of **9** (with a p-OH on the A-ring), indicating possible favourable interactions involving hydrogen bonding in the B-ring.

We also explored the impact of the size of the B-ring moiety by introducing a bulky naphthyl (**21**) or biphenyl (**22**) moiety. Both compounds showed similar affinity for CXCR4 ($pIC_{50} = 6.3$). It is noted that the biphenyl analogue **22** fully displaces ^{125}I-CXCL12 binding to CXCR4 (Table 1, Fig. 3). Interestingly, only a small number of the compounds in Table 1 show a full displacement of the chemokine radioligand, most notably **15**, **20** and **22**. These ligands show reasonable diversity in the B-ring while other close analogues do not fully displace the radioligand. This shows that the very subtle pharmacological differences cannot be explained by SAR or by molecular modelling (*vide infra*). A focused positional scan of the B-ring with either a Cl- or methyl-moiety was undertaken (**23**–**28**). All six analogues showed slightly lower level of displacement (62–80%) compared to the unsubstituted analogue **13** (87%). The *p*-

chloro (**23**) and *p*-methyl (**24**) analogues show a decrease in binding affinity and LLE. The *o*-chloro (**25**), *o*-methyl (**26**) and *m*-chloro (**27**) substituted analogues possess comparable affinities ($pIC_{50} = 6.7$, 6.6 and 6.5, respectively) to **13**. Encouragingly, the *m*-methyl analogue (**28**) shows a pIC_{50} value of 6.8 with, however, a partial displacement (63%) of ^{125}I-CXCL12 binding (Table 1, Fig. 3). Substitution on the *meta* position on the B-ring was deemed preferred within the *o*-chlorosubstituted A-ring series. To re-examine the role of the position of the chlorine substituent on the A-ring with a *meta*-methyl substituted B-ring, we synthesised positional analogues of **28** (**29**, **30**) as well as selected dichloro derivatives (**31**, **32**). The loss of affinity for both, the *m*-chloro (**29**) and *p*-chloro (**30**) substituted analogues (pIC_{50} 5.6 and 5.0, respectively), confirms an important role for the *ortho* substitution of chlorophenyl group. The results also revealed that a 2,3-disubstituted dichloro analogue (**31**) is less potent ($pIC_{50} = 6.1$) compared to **28**, whereas the 2,6-disubstituted isomer (**32**) is equipotent to **28.** However, both disubstituted analogues possess lower LLE (0.28 and 0.67) compared to **28** (LLE = 1.59) due to the increased lipophilicity.

2.4. Pharmacology of key compounds

A concise set of key compounds (**13, 22** and **28**) was selected for further pharmacological analysis. Compounds **13** and **28** display the highest ligand efficiency (LE = 0.39) within the series while all three compounds differ in maximum level of displacement of ^{125}I-CXCL12 binding to hCXCR4. *o*-Chloro substitution on the A-ring together with *m*-phenyl (**22**) or *m*-methyl (**28**) substitution on the B-ring showed a positive effect on binding affinity ($pIC_{50} = 6.3$ and 6.8, respectively) but a remarkably different level of maximal ^{125}I-CXCL12 displacement (98 and 63%, respectively). Within this key set of three, the radioligand displacement results were found to correlate with the results obtained from complementary NanoBRET binding measurements for the displacement of the binding of fluorescently labelled CXCL12-red (25 nM) to NLuc-tagged CXCR4 by the key ligands (Fig. 3B). The binding affinities and the displacement (%) values are combined in Table S1.

The different levels of ^{125}I-CXCL12 displacement as observed for **22** and **28** indicate distinct interactions of the two small molecules with CXCR4. Therefore, we assessed the antagonistic properties of the three ligands (**13**, **22** and **28**) and the reference antagonist AMD3100 against CXCL12-induced CXCR4 activation. In the presence of multiple (0−100 μM) concentrations of the ligand, AMD3100 and **13** (Fig. 4A and B) inhibit the CXCL12-induced G protein activation by CXCR4 in a competitive manner, most likely indicating orthosteric interaction with CXCL12. In contrast, compounds **22** and **28** both show non-competitive antagonistic effects on CXCL12-induced CXCR4 activation (Fig. 4C and D). Interestingly, in the binding study (Fig. 3A) their effect on the inhibition of ^{125}I-CXCL12 binding to CXCR4 differ: compound **22** fully inhibits (98%) ^{125}I-CXCL12 binding (relative to IT1t = 100%), whereas **28** is a partial displacer showing 63% inhibition (Table 1). Thus, amongst the series of CXCR4 ligands, we have found both competitive and non-competitive antagonists including full and partial displacers of CXCL12 binding.

The set of key ligands together with positive control IT1t and the low-affinity ligand **9** as negative control were evaluated in additional functional assays (β-arrestin 2 and Inositol phosphate accumulation). CXCR4-mediated G_i signalling in response to 10 nM CXCL12 was redirected to the phospholipase C − inositol triphosphate ($InsP_3$) pathway by co-expression of the chimeric $G_{\alpha q/i5}$ protein (Fig. 5A), as previously described [52]. Key compounds **13**, **22** and **28** completely inhibited this CXCL12 induced $InsP_3$ formation in a concentration-dependent manner with comparable pIC_{50} values (Table 2). As expected, compound **9** did not significantly inhibit CXCL12-induced signalling in this assay. In line, key compounds **13**, **22** and **28** displayed similar pIC_{50} values in inhibiting β-arrestin 2 recruitment to hCXCR4 in response to 10 nM CXCL12 as measured in a BRET-based assay (Fig. 5B and Table 2). Compound **9** had >10-fold lower pIC_{50} value, which is in line with its lower ability to inhibit ^{125}I-CXCL12 binding as compared to compounds **13**, **22** and **28**.

Taken together, these results demonstrate that despite the distinct displacement of CXC12 binding to CXCR4 (Fig. 3A and B) and being either competitive or non-competitive antagonists (Fig. 4) of CXCL12 signalling *via* CXCR4, compounds **13**, **22** and **28** can be functionally considered full antagonists of CXCR4 chemokine mediated signalling *via* both G_i proteins and β-arrestin2.

2.5. CXCR4 structure-based SAR map

The experimentally determined pIC_{50} values were used to construct 3D-QSAR models in order to identify ligand-based interaction hot spots and prioritize CXCR4-ligand binding mode models (Fig. 6). CXCR4 binding mode models of **28**, based on the two initial binding modes proposed for the experimentally validated virtual screening hit **2** (Fig. 2D and E) were refined by MD simulations, yielding two distinct ligand conformations (Fig. S2) that were used to build the 3D-QSAR models. Both reference ligand conformations provide templates to construct predictive 3D-QSAR models with similar regression and predictive squared correlation coefficients for model 1 ($R^2 = 0.81$, $q^2 = 0.76$, Fig. 6A) and model 2 ($R^2 = 0.80$, $q^2 = 0.71$, Fig. 6D). Fig. 6B and E shows that both models are based on three hydrophobic hotspots defined by the GRID C1 = probe [53,54], including one LB interaction hotspot associated with chemical variations around the A-ring of **28** (LB hot spots 1.1 and 2.1), and two hotspots associated with variations around the B-ring of **28** (LB hot spots 1.2/1.3 and 2.2/2.3). We used the consistency between ligand-based and protein-based interaction models [49] as a complementary criterion to compare ligand binding mode models 1 and 2 (Fig. 6C,F). The 3D-QSAR model based on binding mode 2 provided a better match between the ligand-based (LB) interaction hot spots 2.2 and 2.3 identified by the 3D-QSAR model (Fig. 6E) and the hydrophobic interaction hot spots identified in the receptor binding site, composed of hydrophobic residues W94$^{2.60}$, V112$^{3.28}$, H113$^{3.29}$ and Y116$^{3.32}$ (Fig. 6F). This druggable binding site has indeed been postulated to involve binding of small-molecule ligands to CXCR4 and other chemokine receptors [5,45]. Two exemplary compounds **13** and **22** were selected for binding mode comparison with co-crystallized ligand IT1t. This analysis shows that both compounds can form ionic and hydrogen bond interactions with key residues D97$^{2.63}$ and E288$^{7.39}$, and can target the hydrophobic area. Compound **13** (Fig. 6G) lacks a methyl moiety which would be located around hot spot 2.2 and 2.3, explaining the lower binding affinity of **13** compared to **28**. However, compound **22** (Fig. 6H) with a hydrophobic phenyl group also shows lower affinity, which might be explained by steric hindrance. The described modelling method, matching ligand and protein interaction hotspots derived from experimentally determined SAR data and molecular interaction field analyses, has previously been successfully applied to the elucidation of experimentally validated structural protein-ligand interactions for histamine receptors [49]. The current study demonstrates its applicability in structure-based ligand refinement for less druggable chemokine receptors binding sites.

3. Conclusions

The current studies explore a fragment-like CXCR4 hit that was identified by virtual fragment screening. Ligand-based SAR studies

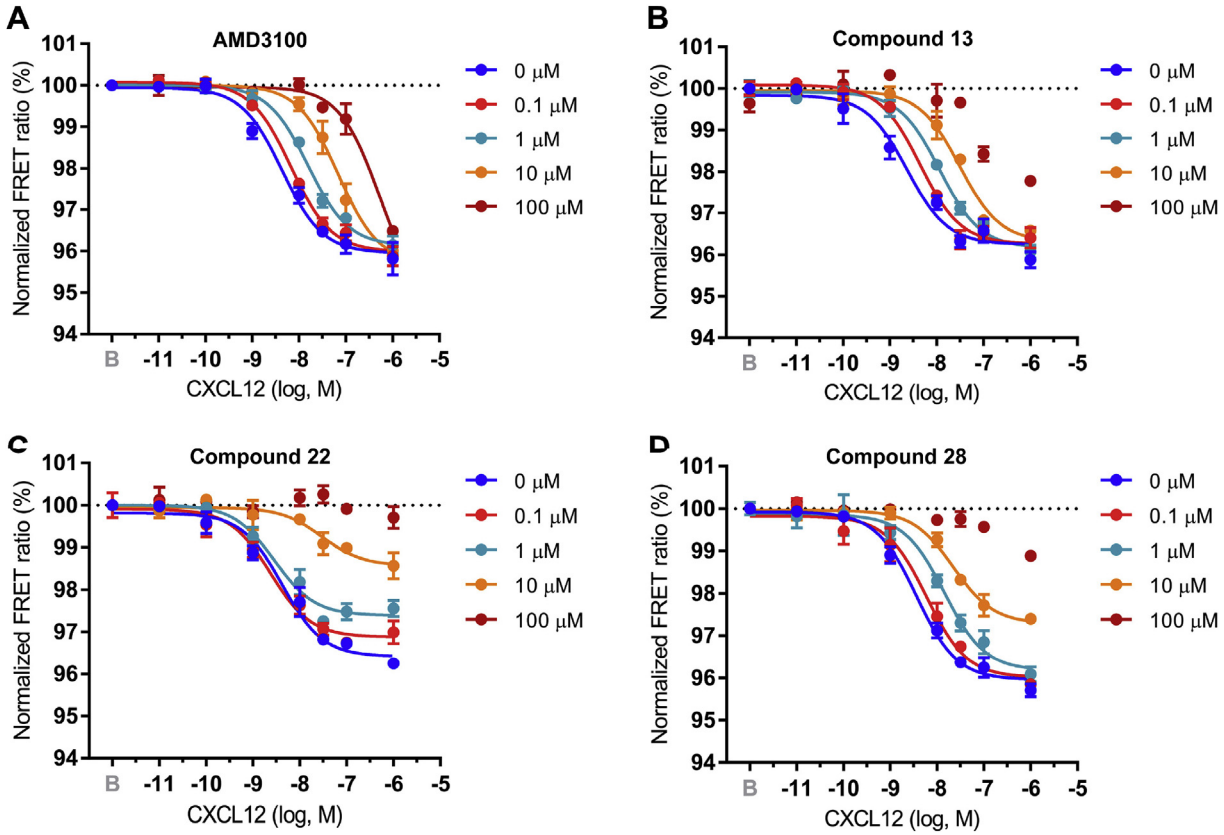


Fig. 4. Evaluation of the effect of key ligands on CXCR4-mediated G protein activation following CXCL12 binding. The concentration-response curves for CXCL12 were determined in the presence of various concentrations of the ligands. G protein activation was measured by pre-incubation of HEK293T cells with increasing concentration of a compound for 30 min followed by addition of CXCL12. Experiments were performed N ≥ 3 with each experiment performed in quadruplicate. (A, B) Competitive behavior by reference antagonist AMD3100 and compound **13**. (C, D) Non-competitive behavior of compounds **22** and **28**.

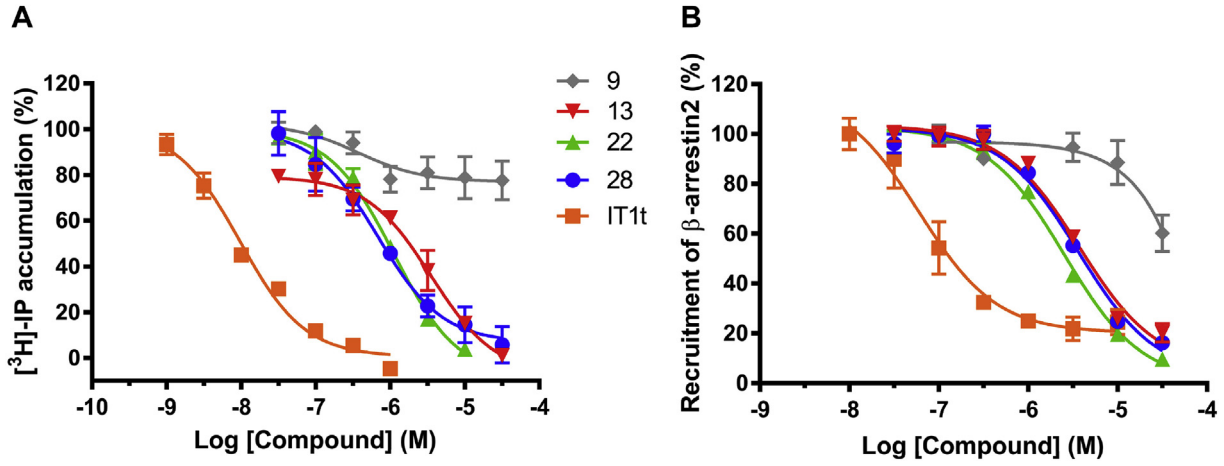


Fig. 5. Inhibition of CXCL12-induced CXCR4 activation by selected compounds. (A) Inhibition of CXCL12-induced $InsP_3$ accumulation in HEK293T cells co-expressing CXCR4 and chimeric $G_{\alpha q/i5}$ proteins by increasing concentration compounds. (B) Inhibition of β-arrestin2 recruitment to CXCR4 in HEK293T cells in response to 10 nM CXCL12 in the presence of increasing concentration compounds or reference IT1t. All experiments were performed N = 3 with each experiment performed in triplicate and mean values ± SEM are shown in Table 2.

were complemented by molecular modelling experiments, including docking and 3D-QSAR studies. This resulted in models that indicate key ligand-receptor interactions. While the models help to explain the affinity and antagonism of the ligands, the observed level of displacement of chemokine CXCL12 binding can so far not be explained by the developed ligand-receptor models, indicating the limitations of fragment-based ligand design to peptidergic GPCRs.

Table 2
Affinity and functional characterization of selected compounds.

Compounds	^{125}I-CXCL12 binding		β-arrestin 2 (BRET)		[^{3}H]-Inositol phosphate accumulation (IPx)	
	pIC_{50}[a]	% displacement[b]	pIC_{50}[a]	% inhibition[b]	pIC_{50}[a]	% inhibition[b]
9	4.5 ± 0.3	65 ± 2	<4.5[c]	N/A[c]	<4.5[c]	N/A[c]
13	6.5 ± 0.1	87 ± 4	5.4 ± 0.0	103 ± 1	5.7 ± 0.2	93 ± 3
22	6.3 ± 0.0	98 ± 1	5.6 ± 0.0	102 ± 6	5.9 ± 0.1	94 ± 3
28	6.8 ± 0.1	63 ± 1	5.5 ± 0.0	97 ± 5	6.0 ± 0.2	87 ± 5
IT1t	8.0 ± 0.0	100 ± 2	7.3 ± 0.0	100 ± 0	7.3 ± 0.0	96 ± 4

[a] Results are means ± SEM (N ≥ 3 with each experiment performed in triplicate).
[b] Results are expressed as percentage of inhibition of CXCL12 binding (50 pM)/signalling (10 nM) by ligand (100 μM) with IT1t as reference (100% inhibition).
[c] pIC_{50} and percentage of inhibition could not be determined.

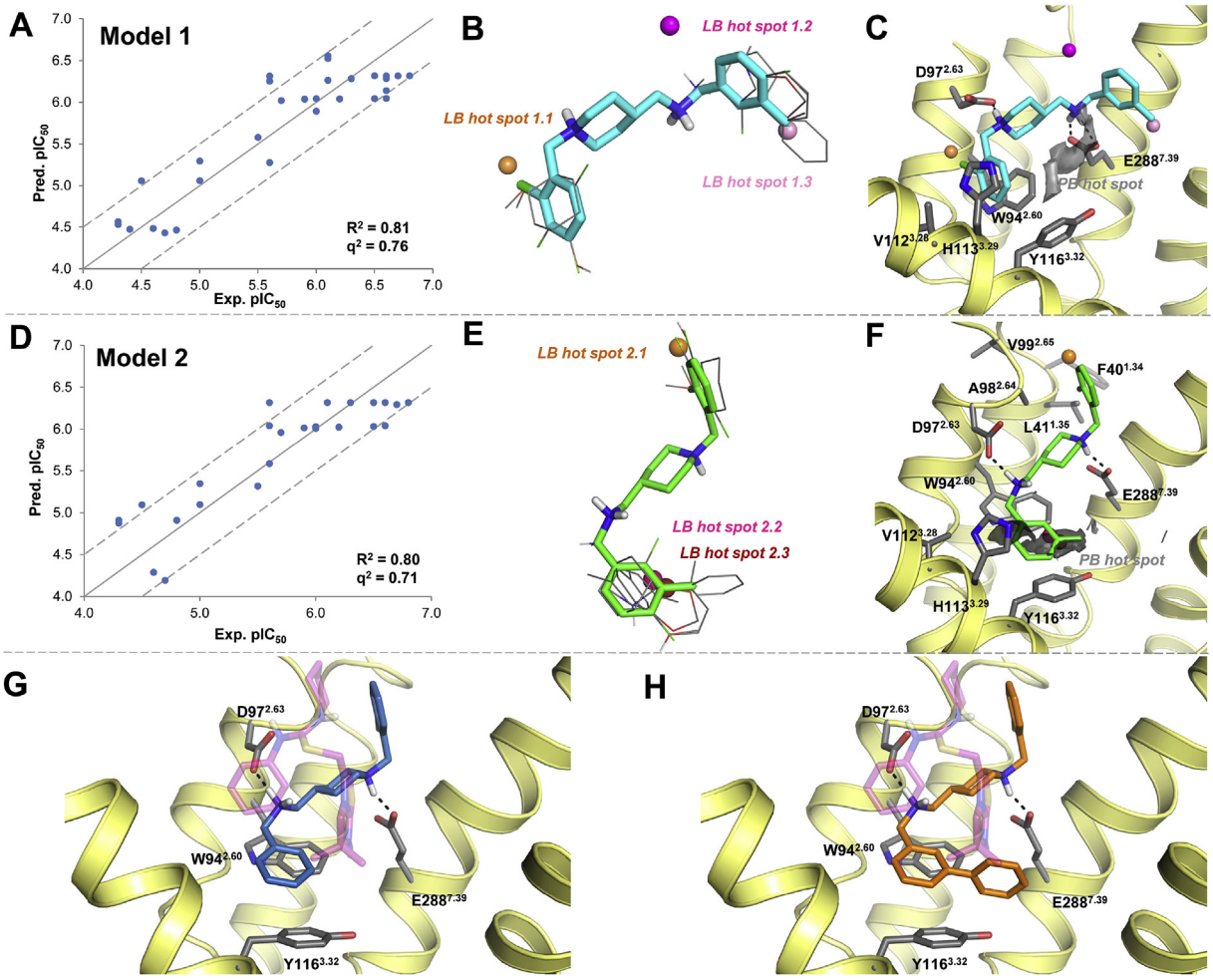


Fig. 6. Details of three-dimensional quantitative structure-activity relationships (3D-QSAR) for Model 1 and Model 2. (A and D) Plot of predicted versus experimental values (pIC_{50}) of Model 1 and Model 2. (B) Alignment of 31 compounds in model 1. Compound **28** is shown in cyan stick, while the others are shown in grey line. The three ligand-based (LB) hot spots are shown in sphere. (C and F) LB 3D-QSAR model aligned with protein-based (PB) hot spots and some key residues (grey stick). Compound **28** is shown in (C) cyan and green (F) stick. Important binding residues are depicted as sticks with grey carbon atoms. Oxygen, nitrogen, and hydrogen atoms are coloured red, blue and white, respectively. H-Bonds described in the text are depicted by dashed lines. (E) Alignment of 31 compounds in model 2. Compound **28** is shown in green stick, while the others are shown in grey line. The three LB hot spots are shown in spheres. (G, H) Plausible binding modes of compounds **13** (dark blue stick) and **22** (orange stick), respectively. Co-crystallized ligand IT1t is shown in transparent magenta stick. (For interpretation of the references to colour in this figure legend, the reader is referred to the Web version of this article.)

4. Experimental

4.1. Computational methods

4.1.1. Residue numbering and nomenclature

The Ballesteros–Weinstein residue numbering scheme [55] was used throughout this manuscript. For explicitly numbered residues in specific receptors, the UniProt residue number is given before the Ballesteros–Weinstein residue number in superscript (e.g., E288$^{7.39}$ in CXCR4).

4.1.2. Preparation of the virtual screening database

We downloaded commercially available compounds from 8 trusted vendors from the ZINC8 database [56] in SMILES format and selected di-cationic 52.500 fragment-like compounds (number of heavy atoms ≤ 22, logP < 3, number of H-bond donors ≤ 3, number of H-bond acceptors ≤ 3, number of rotatable bonds ≤ 5, number of rings ≥ 1) from this set [57,58] using Openeye's filter tool [59]. We selected di-cationic compounds based on the experimentally supported binding mode hypothesis that ionic interactions with residues D97$^{2.63}$ and E288$^{7.39}$ play an important role in CXCR4 binding. The major protonation states of small molecules were computed with ChemAxon Calculators [60] at pH 7.4 and converted to Mol2 format with Molecular Networks' CORINA [61].

4.1.3. Automated docking

The CXCR4 crystal structure (PDB.: 3ODU) was prepared for docking simulations using the MOE [62] Protonate3D module in order to ensure a plausible ionization state for each residue, followed by visual inspection. Docking experiments were performed with the programs GOLD [42] and PLANTS [43], using the crystal structure of CXCR4 (3ODU) [6]. PLANTS combines an ant colony optimization algorithm with an empirical scoring function [63] for the prediction and scoring of binding poses in a protein structure. GOLD is an automated ligand docking program that uses a genetic algorithm to explore the full range of ligand conformational flexibilities with partial flexibility of the protein. For each compound, 15 poses were calculated, and scored by the *ChemPLP* scoring function at speed setting 2 in PLANTS. All other options of PLANTS were left at their default setting. We performed 15 GA runs for each ligand in GOLD and the population size was set to 100 (selection pressure 1.1, number of islands 3, maximum number of operation per ligands 3000 and niches size 2); For flags, internal H-bonds and planar trigonal nitrogen flipping were enabled, and restricted ligand conformational space by torsion angle distributions from CSD. The genetic operators (pt_crosswt = 95, allele_mutatewt = 95, migratewt = 10) and other options were kept as default. The docking poses were sorted by *GoldScore* fitness function. The binding pocket of CXCR4 was defined by the coordinates of the center of co-crystallized IT1t in the 3ODU structure and a radius of 5 Å (which is the maximum distance from the center defined by a 5 Å radius around IT1t).

4.1.4. IFP post-processing

Structural interaction fingerprint analysis [44,64,65] was used for post-processing of docking poses in structure-based virtual screening studies. The IT1t binding mode in the original CXCR4 X-ray structure [6] (PDB code 3ODU) was used to generate reference structural interaction fingerprints (IFPs) as previously described [44]. Seven different interaction types (hydrophobic, aromatic face-to-edge, aromatic face-to-face, H-bond acceptor, H-bond donor, negatively charged, and positively charged interactions) were used to define the IFP. The cavity used for the IFP analysis consisted of the same binding pocket used for docking, including E32$^{1.26}$, K38$^{1.32}$, L41$^{1.35}$, Y45$^{1.39}$, F93$^{2.59}$, W94$^{2.60}$, D97$^{2.63}$, A98$^{2.64}$, W102$^{23.50}$, C109$^{3.25}$, V112$^{3.28}$, H113$^{3.29}$, Y116$^{3.32}$, L120$^{3.36}$, D171$^{4.60}$, R183$^{45.47}$, I185$^{45.49}$, C186$^{45.50}$, D187$^{45.51}$, R188$^{45.52}$, Y255$^{6.51}$, H281$^{7.31}$, S285$^{7.35}$, E288$^{7.39}$, F292$^{7.42}$. Standard IFP scoring parameters, and a Tanimoto coefficient (Tc-IFP) [44] measuring IFP similarity with the reference molecule pose (IT1t in the CXCR4 crystal structure 3ODU, Fig. 2B), was used to filter and rank the docking poses of the 52.500 fragment-like compounds in the virtual screening library. Only poses forming an H-bond and ionic interaction with residues D97$^{2.63}$ and E288$^{7.39}$ were considered.

4.1.5. Structure-based virtual screening

The screening database was docked with PLANTS and GOLD, and resulting docking poses were post-processed using IFP analysis and filtered for ionic and H-bond interactions with D97$^{2.63}$ and E288$^{7.39}$. IFP (Tc ≥ 0.75) and PLANTS (≤−90) scoring cut-offs derived from previously GPCR structure-based virtual screening on H_1R [65] were used to select a total of 1.917 compounds. This set was clustered and compared to known CXCR4 ligands in ChEMBL using ECFP-4 (extended connectivity fingerprints) [66] descriptors available in KNIME analytics platform [67] and compared using the Tanimoto coefficient. The docking poses of well-populated chemical clusters of hit molecules were visually inspected in more detail, and those molecules that targeted the hydrophobic hot spot in the minor binding site were prioritized. This yielded a final set of 34 hit molecules of which 23 were purchased and experimentally tested.

4.1.6. MD simulations

Docking studies on compound **28** revealed two alternative binding models and both can target D97$^{2.63}$ and E288$^{7.39}$ simultaneously. The two distinguished models of the hit compound **28** bound to CXCR4 were energy minimized for 1000 steps and used to run membrane-embedded MD simulations in GROMACS [68]. Each system was simulated for 100 ns after an equilibration of 5 ns in which positional restraints were gradually relaxed in order to allow lipids to properly adapt around the protein and to allow water molecules to fill up receptor cavities. The trajectories were generated unrestrained with the parameters and conditions described elsewhere [69]. The parameters of the ligands were obtained using the General Amber Force Field 2 (GAFF2) and AM1-BCC HF/6-31G* ESP fitted atomic charges [70] were used. Potential energy, RMSD, RMSF, and dihedrals of the simulations were analyzed with GROMACS tools. The major protonation state of the 31 small molecules were computed with ChemAxon's Calculators [60] at pH 7.4.

4.1.7. 3D-QSAR

The two refined 3D structures of compound **28** derived from MD simulations were used as templates and other molecules were sketched and refined using MOE [71] as previously described. The MIF probes (DRY and C1 =) were then calculated using the GRID package (version 22 from Molecular Discovery) [72]. The probes in a radius of 5 Å around aligned compounds were calculated using a grid resolution of 0.5 Å. The values of the probes were normalized, and probes with standard deviation of less than 1.0 or correlation less than 0.3 were filtered out by employing R statistical package (version 2.7.1) [73]. The Genetic method followed by GreedyStepwise method from Weka 3.8 data-mining software package [74] were subsequently used to automatically select the important probes and generate QSAR models, with dependent variables being pIC_{50} of CXCR4.

4.2. Pharmacology

4.2.1. Cell culture

Human embryonic kidney 293T cells (HEK293T) were grown at 37 °C and 5% CO_2 in Dulbecco's modified Eagle medium (Gibco) supplemented with 10% fetal bovine serum (Bodinco), penicillin-streptomycin (Gibco).

4.2.2. CXCR4 membrane preparation

CXCR4-expressing HEK293T cell membranes were prepared as previously described [75]. HEK293T cells ($2 \cdot 10^6$) were seeded in a 10-cm dish and transfected the next day. The medium of the cells was refreshed using 8 mL of culture medium. 5 μg of pcDEF$_3$-hCXCR4 was combined with 40 μg of PEI in a total volume of 500 μL 150 mM NaCl and incubated for 20 min at room temperature.

Subsequently, the DNA/PEI mix was added to the cells. Two days after transfection, cells were collected in ice-cold PBS and centrifuged at 1500 g for 10 min at 4 °C. Subsequently, cells were washed with PBS and centrifuged at 1500 g for 10 min at 4 °C. The pellet was resuspended in ice-cold membrane buffer (15 mM Tris pH 7.5, 1 mM EGTA, 0.3 mM EDTA, 2 mM $MgCl_2$) and homogenized by 10 strokes at 1100–1200 rpm using a teflon-glass homogenizer and rotor. The membranes were subjected to two freeze thaw cycles using liquid nitrogen and centrifuged at 40,000 g for 25 min at 4 °C. The pellet was resuspended in cold Tris-sucrose buffer (20 mM Tris pH 7.4, 250 mM sucrose), and frozen in liquid nitrogen. Protein concentration was determined using a BCA protein assay kit (Thermo Fisher).

4.2.3. ^{125}I-CXCL12 binding assay

CXCR4 membranes (5 μg/well) were incubated in 96-well clear plates (Greiner Bio One, PS, U-bottom, clear) in binding buffer (50 mM HEPES, pH 7.4, 1 mM CaCl2, 5 mM MgCl2, 100 mM NaCl, and 1.0% (w/v) bovine serum albumin (BSA, fraction V)) with approximately 50 pM ^{125}I-CXCL12 (PerkinElmer) in the absence or presence of unlabeled ligands for 2 h at 25 °C with gentle agitation. The incubations were terminated by rapid filtration through Unifilter 96-well GF/C plates (PerkinElmer) presoaked with 0.5% PEI using ice-cold wash buffer (binding buffer supplemented with 0.5 M NaCl) to separate free from bound radioligand. The filter plates were dried at 52 °C and 25 μl Microscint-O was added. Bound radioactivity was quantified with a MicroBeta scintillation counter (PerkinElmer). Data was analyzed using the GraphPad Prism 7 software. Non-linear regression curves were fitted using the "log(inhibitor) vs. response (three parameters)" equation. Percentage displacement of ^{125}I-CXCL12 was calculated with controls present on each plate (10^{-5} M IT1t (Tocris) for determining non-specific binding: NS, vehicle treated for determining total binding: TB) following this equation: (X-NS)/(TB-NS)x100.

4.2.4. Bioluminescence resonance energy transfer (BRET) β-arrestin recruitment assay

0.4 μg of pcDEF$_3$-hCXCR4-RLuc (as previously described) [76] and 1.6 μg pcDEF$_3$-β-arrestin-2-mVenus (as previously described) [77] plasmids were combined to 12 μg of PEI in a total volume of 250 μL 150 mM NaCl and incubated for 20 min at room temperature. 1 million resuspended HEK293T cells were added to the DNA/PEI mix, and cells were subsequently seeded (30,000 cells per well) on 96-well white plate (Greiner Bio One, PS, F-bottom, white). Two days after transfection, culture medium was substituted with Hanks' balanced salt solution (Gibco). Next, cells were pre-incubated in Hanks' balanced salt solution with increasing concentrations of compound for 60 min before stimulation with 10 nM CXCL12 and addition of 5 μM Renilla Luciferase substrate coelenterazine-h (Promega). After 20 min, RLuc (480/20 nm) and BRET (540/40 nm) signals were measured on the Mithras LB940 (Berthold Technologies). BRET ratios were calculated as BRET signal over RLuc signal, and fold over vehicle was determined using controls.

4.2.5. Inositol phosphate (IP) accumulation assay

HEK293T cells ($2 \cdot 10^6$) were seeded in a 10-cm dish and transfected the next day. The medium of the cells was refreshed using 8 mL of culture medium. 5 μg of DNA including pcDEF3-CXCR4 and pcDNA1-HA-$G_{\alpha q/i5}$ [52] was combined with 40 μg of PEI in a total volume of 500 μL 150 mM NaCl and incubated for 20 min at room temperature. Subsequently, the DNA/PEI mix was added to the cells. The next day, cells were transferred to ($120 \cdot 10^3$/well) a poly-L-lysine (Sigma) coated 48-wells plate and were incubated overnight in DMEM inositol-free medium (MP) supplemented with 1 μCi/mL [^{3}H]-myo-inositol (PerkinElmer). Cells were then treated with or without a dilution range of antagonist in buffer (20 mM HEPES, 140 mM NaCl, 5 mM KCl, 1 mM $MgSO_4$, 1 mM $CaCl_2$, 10 mM D-(+)-Glucose, pH 7.4) with 10 nM CXCL12 and 10 mM LiCl and 0.05% BSA for 1.5 h at 37 °C. Cells were lysed and the accumulated inositol phosphates (InsP3) were isolated using affinity purification columns (Bio-Rad). The amount of radiolabeled IP was determined after the addition of a scintillation fluid (PerkinElmer) on a Tri-Carb 2800TR (PerkinElmer).

4.2.6. Fluorescence resonance energy transfer (FRET) G protein activation assay

To test G protein activation, the previously described $G_{\alpha i1}$ FRET-based sensor and the untagged human CXCR4 receptor in pcDEF3 was used [78]. The G protein sensor contains all three subunits of the G protein in a single plasmid: the α_{i1} subunit fused to mTurquoise-Δ9, the β1 subunit and the γ2 subunit fused to cp173Venus (pGβ1-2A-cp173Venus-Gγ2-IRES-Gαi1-mTurquoise2-Δ9).
HEK293T cells were cultured at the University of Wuerzburg (Wuerzburg, Germany) using Dulbecco's Modified Eagle Medium (DMEM) supplemented with 4.5 g/l glucose, 10% (v/v) fetal calf serum, 100 U/mL penicillin G, and 100 μg/mL streptomycin sulphate and L-glutamine (2 mM) at 37 °C and 7% CO_2. To investigate G protein activation, HEK293T cells were seeded in 100 mm plates and allowed to grow until the cells reached 60–65% confluency. At this stage, cells were transiently transfected with the Effectene transfection reagent (Qiagen), according to the manufacturer's instructions. For transfection, the following DNA amounts were used per plate: 1.4 μg of CXCR4 receptor and 3 μg of $G\alpha_{i1}$ sensor. As a control, empty vector plasmid was used. 24 h after transfection, black 96 well BRAND-plates (flat bottom) were coated with 90 μL poly-D-lysine (1 mg/mL) for 30 min. Next, poly-D-lysine was aspirated and each well was washed once with 200 μL of PBS. Transfected HEK293T cells were harvested by 2 min treatment with 1 mL trypsin solution and cells were resuspended in culture media and counted. Cells were seeded at a density of 30,000 cells per well. On the day of the measurement, the medium of the cells was removed and 90 μL of measuring buffer (140 mM NaCl, 5.4 mM KCl, 2 mM $CaCl_2$, 1 mM $MgCl_2$, 10 mM HEPES, pH 7.3) was added to the cells and incubated at 37 °C during 30 min. Analysis of the cells was done 24 h after seeding the cells in the 96-well plates using Synergy™ Neo2 Multi-Mode Microplate Reader (Biotek) with Gen5™ Data Analysis Software. During the measurement, cells were illuminated at 420/50 nm (Biotek CFP-YFP Filter; 1035013) and emission was monitored at 485/20 nm and 540/25 nm (Biotek CFP-YFP Filter; 1035043). The fluorescence was read during 5 min to determine the pre-read signal. Following the pre-read measurement, 10 μL of increasing concentrations of CXCL12 was added to the wells for a total assay volume of 100 μL. Fluorescence was read again during 20 min to determine the post-read signal. During measurement, cells were kept at 37 °C. Data were analyzed using the software GraphPad Prism 6. To study the effect of the antagonists on G protein activation, the same procedure was applied, but modified in the following way. Before the measurement, the test compounds, initially dissolved in DMSO, were diluted in measuring buffer to reach a final assay concentration of 100 μM, 10 μM, 1 μM or 0.1 μM. Cells were pre-incubated at 37 °C during 30 min with 90 μL of buffer containing the corresponding antagonist concentration. After 5 min of reading, G protein activation was then stimulated as described above by adding an additional 10 μL solution of increasing concentrations of CXCL12 and measuring for additional 20 min. For each antagonist, 3 to 5 repetitions were performed. To confirm that the different concentrations of DMSO do not affect the results, G protein activation was tested in the presence of 0%, 0.001%, 0.01%, 0.1% and 1% of DMSO in measuring buffer.

4.2.7. BRET CXCL12-red binding assay

A pcDNA3.1 plasmid containing the Nanoluc (Nluc) - labelled CXCR4 receptor was created from a previously described construct by replacing the adenosine-A_1 receptor cDNA with that encoding the human CXCR4 [79]. The final construct encoded a fusion of sig-Nluc, a Gly-Ser linker and CXCR4 with the methionine start signal removed. Mixed-population HEK293G cell lines (Glosensor cAMP HEK293, from Promega) were created by transfecting cells with the Nluc–CXCR4 receptor construct using FuGENE® (Promega) according to the manufacturer's instructions and then subjecting cells to selective pressure (1 mg/mL G418) for 2–3 weeks. HEK293G cells were maintained in Dulbecco's modified Eagle's medium (DMEM) containing 10% fetal calf serum (FCS) and 2 mM L-glutamine at 37 °C, 5% CO_2. Membranes for NanoBRET binding assays were prepared from HEK293-Nluc-CXCR4 cells as previously described [80]. Competition NanoBRET binding assays were performed essentially as described previously [80]. Briefly, membranes were diluted to 10 μg protein/well in HEPES buffered saline solution (HBSS, 25 mM HEPES, 10 mM glucose, 146 mM NaCl, 5 mM KCl, 1 mM $MgSO_4$, 2 mM sodium pyruvate, 1.3 mM $CaCl_2$, pH 7.4) and placed in white Thermo Scientific 96-well microplates prior to addition of compounds. 50 nM CXCL12-red (ALMAC, Edinburgh, UK) and increasing concentrations of competing ligand were added simultaneously. Plates were then incubated for 2 h at 37 °C when 10 μM furimazine (Promega) was added to each well and luminescence emission measured after 5min using a PHERAstar FS plate reader (BMG Labtech) at room temperature. Filtered light emissions were measured at 460 nm (80-nm bandpass) and at > 610 nm (longpass) and the raw BRET ratio was calculated by dividing the >610-nm emission by the 460-nm emission.

4.3. Chemistry

4.3.1. Materials and methods

Commercial reagents and solvents were used without further purification. Dry solvents (THF, DCM) were obtained from PureSolv solvent purification system by Inert®. All reactions were carried out under an inert N_2 atmosphere unless otherwise stated. TLC analyses were performed with Merck F254 Alumina Silica Plates using UV visualization or staining. Column purifications were carried out automatically using Isolera One Biotage® equipment. ^1H and ^{13}C (incl. 2D-NMR) spectra were recorded on a Bruker spectrometer with operating frequency 250 MHz, 500 MHz 600 MHz and 63 MHz, 126 MHz and 151 MHz, respectively. NMR spectra were calibrated according to internal references for non-deuterated solvents: $CHCl_3$ ($\delta_H = 7.26$ ppm), $CDCl_3$ ($\delta_C = 77.16$ ppm), DMSO ($\delta_H = 2.50$), DMSO-d_6 ($\delta_C = 39.52$ ppm) and H_2O ($\delta_H = 4.79$). The following abbreviations were used to denote multiplicities: s = singlet, d = doublet, t = triplet, q = quartet, m = multiplet, dd = doublet of doublets, dt = doublet of triplets, td = triplet of doublets, qd = quartet of doublets, br = broad signal, app = apparent. Systematic names for molecules according to IUPAC rules were generated using ChemDraw Pro 16.0. Melting trajectories for compounds **9**, **20**–**22** and **27** were determined using Buchi M-565 melting point apparatus with the rate of 1 °C/min. All HRMS spectra were recorded on Bruker microTOF-Q MS using ESI in positive ion mode. Unless specified otherwise, all compounds have a purity ≥95% that was determined using a Shimadzu HPLC/MS workstation with a LC-20AD pump system, SPD-M20A diode array detection and a LCMS-2010 EV Liquid Chromatograph Mass Spectrometer and applying either a basic or acidic mode. Compound purities were calculated as the percentage peak area of the analyzed compound by UV detection at, unless stated otherwise, 230 nm. The column used is an Xbridge C18 5 mm column (50 mm × 4.6 mm). *Basic mode:* Solvent B (MeCN/10% buffer), Solvent A (water/10% buffer). The buffer is a 0.4% (w/v) NH_4HCO_3 solution in water, adjusted to pH 8.0 with NH_4OH. The analysis was conducted using a flow rate of 1.0 mL/min with a total run time of 8 min or 12 min depending on the lipophilicity of the analyte. *Acidic mode*: For compounds **6b** and **6f** an acidic solvent system was used: Solvent B (MeCN/0.1% formic acid) and solvent A (water/0.1% formic acid), flow rate of 1.0 mL/min with a run time of 8 min. *Gradient settings*: For 8 min run (basic and acidic system): start 5% B, linear gradient to 90% B in 4.5 min, then isocratic for 1.5 min at 90% B, then linear gradient to 5% B in 0.5 min, then isocratic for 1.5 min at 5% B. For 12 min run (basic system): start 5% B, linear gradient to 90% B in 4.5 min, then 5.5 min at 90% B, then linear gradient to 5% B in 0.5 min, then isocratic for 1.5 min at 5% B.

4.3.2. Synthesis

4.3.2.1. General procedure A. Direct reductive amination. $NaBH(OAc)_3$ (typically 1.4 eq) was added to a solution of amine **5** (typically 1.0 eq) and aldehyde (typically 1.0 eq) in 1,2-dichloroethane (DCE). The mixture was stirred at rt until the conversion was finished as judged by TLC and LC/MS analyses. The reaction mixture was quenched with 10% K_2CO_3 aqueous solution. The product was extracted with dichloromethane (DCM) (3x). The combined organic layers were washed with brine (1x). Subsequently, the organic layer was dried with anhydrous Na_2SO_4. The solvent was removed *in vacuo* to give crude product which was purified by flash column chromatography. Unless mentioned otherwise, cyclohexane/5% TEA: EtOAc/5%TEA and a gradient flow from 100-0% to 50-50% were used.

The compounds **6a,b,d-l** were prepared according to the general procedure A.

*4.3.2.1.1. Tert-butyl ((1-(2-chlorobenzyl)piperidin-4-yl)methyl) carbamate **(6a)**.* The general procedure A was followed using *tert*-butyl-(piperidin-4-ylmethyl)carbamate (**5a**) (3.210 g, 15.00 mmol), 2-chlorobenzaldehyde (2.140 g, 15.00 mmol), $NaBH(OAc)_3$ (4.590 g, 21.00 mmol), DCE (50 mL) and a reaction time of 20 h. Compound **6a** was obtained as a white solid (3.980 g, 78%). ^1H NMR (250 MHz, $CDCl_3$) δ 7.47 (d, J = 7.3 Hz, 1H), 7.33 (dd, J = 7.5, 1.8 Hz, 1H), 7.25–7.13 (m, 2H), 4.59 (s, 1H), 3.60 (s, 2H), 3.02 (app t, J = 6.3 Hz, 2H), 2.91 (app d, J = 11.6 Hz, 2H), 2.06 (app t, J = 11.4 Hz, 2H), 1.66 (app d, J = 12.8 Hz, 2H), 1.48–1.39 (m, 10H), 1.37–1.21 (m, 2H). ESI-MS *m/z:* 339.00 $[M + H]^+$.

*4.3.2.1.2. Tert-butyl ((1-(3,4-dichlorobenzyl)piperidin-4-yl) methyl)carbamate **(6b)**.* The general procedure A was followed using **5a** (3.210 g, 15.00 mmol), 3,4-dichlorobenzaldehyde (2.760 g, 15.00 mmol), $NaBH(OAc)_3$ (4.590 g, 21.00 mmol), DCE (50 mL) and a reaction time of 17 h. Compound **6b** was obtained as a white solid (4.480 g, 78%). ^1H NMR (250 MHz, $CDCl_3$) δ 7.41 (d, J = 2.0 Hz, 1H), 7.36 (d, J = 8.2 Hz, 1H), 7.14 (dd, J = 8.2, 2.0 Hz, 1H), 4.61 (s, 1H), 3.41 (s, 2H), 3.01 (app t, J = 6.3 Hz, 2H), 2.83 (app d, J = 11.6 Hz, 2H), 1.93 (app t, J = 11.5 Hz, 2H), 1.74–1.60 (m, 2H), 1.53–1.38 (m, 10H), 1.32–1.16 (m, 2H). ESI-MS *m/z*: 372.95 $[M + H]^+$.

*4.3.2.1.3. Tert-butyl ((1-(2-methoxybenzyl)piperidin-4-yl)methyl) carbamate **(6d)**.* The general procedure A was followed using **5a** (3.210 g, 15.00 mmol), 2-methoxybenzaldehyde (2.04 g, 15.00 mmol) and $NaBH(OAc)_3$ (4.590 g, 21.00 mmol), DCE (50 mL) and a reaction time of 20 h. Compound **6d** was obtained as a white solid (3.507 g, 71%). ^1H NMR (500 MHz, $CDCl_3$) δ 7.34 (d, J = 7.4 Hz, 1H), 7.22 (t, J = 7.8 Hz, 1H), 6.92 (t, J = 7.4 Hz, 1H), 6.86 (d, J = 8.2 Hz, 1H), 4.59 (d, J = 6.3 Hz, 1H), 3.81 (s, 3H), 3.54 (s, 2H), 3.01 (app t, J = 6.1 Hz, 2H), 2.93 (app d, J = 11.4 Hz, 2H), 2.00 (app t, J = 11.5 Hz, 2H), 1.64 (app d, J = 12.5 Hz, 2H), 1.48–1.39 (m, 10H), 1.32–1.26 (m, 2H). ESI-MS *m/z*: 335.20 $[M + H]^+$.

*4.3.2.1.4. Tert-butyl ((1-(cyclohexylmethyl)piperidin-4-yl)methyl) carbamate **(6e)**.* The general procedure A was followed using **5a** (0.560 g, 2.50 mmol), cyclohexanecarbaldehyde (0.290 g,

2.50 mmol) and $NaBH(OAc)_3$ (0.780 g, 3.50 mmol), DCE (10 mL) and a reaction time of 3 days. Compound **6e** was obtained as a white solid (0.82 g, 76%). ^1H NMR (250 MHz, $CDCl_3$) δ 4.60 (s, 1H), 2.99 (app t, J = 6.1 Hz, 2H), 2.84 (app d, J = 11.7 Hz, 2H), 2.07 (d, J = 7.0 Hz, 2H), 1.88–1.56 (m, 9H), 1.43 (s, 11H), 1.34–1.06 (m, 5H), 0.95–0.71 (m, 2H). ESI-MS m/z: 311.20 $[M + H]^+$.

*4.3.2.1.5. Tert-butyl (2-(1-(2-chlorobenzyl)piperidin-4-yl)ethyl) carbamate **(6f)**.* The general procedure A was followed using **5b** (0.300 g, 1.31 mmol), 2-chlorobenzaldehyde (0.190 g, 1.31 mmol), $NaBH(OAc)_3$ (0.400 g, 1.84 mmol), DCE (5 mL) and a reaction time of 6 days. Compound **6f** was obtained as a white solid (0.330 g, 72%). ^1H NMR (250 MHz, $CDCl_3$) δ 7.43 (dd, J = 7.4, 2.0 Hz, 1H), 7.29 (dd, J = 7.6, 1.6 Hz, 1H), 7.22–7.07 (m, 2H), 4.68 (s, 1H), 3.54 (s, 2H), 3.10 (app q, J = 6.7 Hz, 2H), 2.93–2.78 (m, 2H), 1.90–2.10 (m, 2H), 1.70–1.56 (m, 2H), 1.48–1.30 (m, 11H), 1.29–1.11 (m, 3H). ESI-MS m/z: 353.00 $[M + H]^+$.

*4.3.2.1.6. Tert-butyl ((1-benzylpiperidin-4-yl)methyl)carbamate **(6g)**.* The general procedure A was followed using **5a** (1.00 g, 4.69 mmol), benzaldehyde (0.500 g, 4.69 mmol) and $NaBH(OAc)_3$ (1.390 g, 6.56 mmol), DCE (20 mL) and a reaction time of 48 h. Compound **6g** was obtained as a white solid (1.400 g, 98%). ^1H NMR (500 MHz, $CDCl_3$) δ 7.32–7.26 (m, 5H), 4.59 (s, 1H), 3.50 (s, 2H), 3.01 (app t, J = 6.4 Hz, 2H), 2.90 (app d, J = 11.0 Hz, 2H), 1.95 (app t, J = 11.7 Hz, 2H), 1.69–1.59 (m, 2H), 1.43 (s, 10H), 1.31–1.25 (m, 2H). ESI-MS m/z: 305.20 $[M + H]^+$.

*4.3.2.1.7. Tert-butyl ((1-(4-hydroxybenzyl)piperidin-4-yl)methyl) carbamate **(6h)**.* The general procedure A was followed using **5a** (2.140 g, 10.00 mmol), 4-hydroxybenzaldehyde (1.220 g, 10.00 mmol) and $NaBH(OAc)_3$ (2.970 g, 14.00 mmol), DCE (50 mL) and a reaction time of 48 h. Compound **6h** was obtained as a yellow solid (2.42 g, 74%). ^1H NMR (500 MHz, $CDCl_3$) δ 7.05 (d, J = 7.9 Hz, 2H), 6.58 (d, J = 8.0 Hz, 2H), 4.68 (t, J = 6.2 Hz, 1H), 3.42 (s, 2H), 3.02–2.88 (m, 4H), 2.00 (app t, J = 11.7 Hz, 2H), 1.66 (app d, J = 13.0 Hz, 2H), 1.54–1.37 (m, 11H), 1.31–1.25 (m, 2H). ESI-MS m/z: 321.15 $[M + H]^+$.

*4.3.2.1.8. Tert-butyl ((1-(4-chlorobenzyl)piperidin-4-yl)methyl) carbamate **(6i)**.* The general procedure A was followed using **5a** (1.07 g, 5.00 mmol), 4-chlorobenzaldehyde (0.700 g, 5.00 mmol) and $NaBH(OAc)_3$ (1.48 g, 7.00 mmol), DCE (20 mL) and a reaction time of 5 days. Compound **6i** was obtained as a white solid (0.67 g, 40%). ^1H NMR (500 MHz, $CDCl_3$) δ 7.29–7.22 (m, 4H), 4.59 (s, 1H), 3.43 (s, 2H), 3.01 (app t, J = 6.5 Hz, 2H), 2.85 (app d, J = 11.3 Hz, 2H), 1.92 (app t, J = 11.5 Hz, 2H), 1.64 (app d, J = 12.9 Hz, 2H), 1.47–1.39 (m, 10H), 1.30–1.21 (m, 2H). ESI-MS m/z: 339.15 $[M + H]^+$.

*4.3.2.1.9. Tert-butyl ((1-(3-chlorobenzyl)piperidin-4-yl)methyl) carbamate **(6j)**.* The general procedure A was followed using **5a** (1.070 g, 5.00 mmol), 3-chlorobenzaldehyde (0.700 g, 5.00 mmol) and $NaBH(OAc)_3$ (1.480 g, 7.00 mmol), DCE (30 mL) and a reaction time of 48 h. Compound **6j** was obtained as a white solid (0.690 g, 41%). ^1H NMR (500 MHz, $CDCl_3$) δ 7.32 (s, 1H), 7.25–7.17 (m, 3H), 4.62 (s, 1H), 3.46 (s, 2H), 3.05–2.92 (m, 2H), 2.87 (app d, J = 11.1 Hz, 2H), 1.95 (app t, J = 11.6 Hz, 2H), 1.66 (app d, J = 12.8 Hz, 2H), 1.48–1.39 (m, 10H), 1.31–1.24 (m, 2H). ESI-MS m/z: 339.15 $[M + H]^+$.

*4.3.2.1.10. Tert-butyl ((1-(2,3-dichlorobenzyl)piperidin-4-yl) methyl)carbamate **(6k)**.* The general procedure A was followed using **5a** (2.140 g, 10.00 mmol), 2,3-dichlorobenzaldehyde (1.750 g, 10.00 mmol) and $NaBH(OAc)_3$ (2.970 g, 14.00 mmol), DCE (60 mL) and a reaction time of 43 h. Compound **6k** was obtained as a white solid (1.220 g, 33%). ^1H NMR (500 MHz, $CDCl_3$) δ 7.40 (d, J = 7.7 Hz, 1H), 7.34 (d, J = 7.9 Hz, 1H), 7.17 (t, J = 7.8 Hz, 1H), 4.59 (s, 1H), 3.59 (s, 2H), 3.02 (app t, J = 6.5 Hz, 2H), 2.92–2.84 (m, 2H), 2.07 (app t, J = 2.3, 11.6 Hz, 2H), 1.70–1.64 (m, 2H), 1.51–1.39 (m, 10H), 1.35–1.21 (m, 2H). ESI-MS m/z: 373.10 $[M + H]^+$.

*4.3.2.1.11. Tert-butyl ((1-(2,6-dichlorobenzyl)piperidin-4-yl) methyl)carbamate **(6l)**.* The general procedure A was followed using **5a** (1.070 g, 5.00 mmol), 2,6-dichlorobenzaldehyde (0.880 g, 5.00 mmol) and $NaBH(OAc)_3$ (1.480 g, 7.00 mmol), DCE (30 mL) and a reaction time of 48 h. Compound **6l** was obtained as a white solid (0.84 g, 45%). ^1H NMR (500 MHz, $CDCl_3$) δ 7.29 (d, J = 7.9 Hz, 2H), 7.13 (br s, 1H), 4.59 (s, 1H), 3.70 (s, 2H), 2.99 (app t, J = 6.5 Hz, 2H), 2.92 (br s, 2H), 2.17 (br s, 2H), 1.61 (br s, 2H), 1.45–1.42 (m, 10H), 1.20 (br s, 2H). ESI-MS m/z: 373.10 $[M + H]^+$.

*4.3.2.1.12. Tert-butyl ((1-(2-methylbenzyl)piperidin-4-yl)methyl) carbamate **(6c)**.* To a stirred suspension of **5a** (1.000 g, 4.67 mmol) and K_2CO_3 (1.289 g, 9.33 mmol) in EtOH (20 mL), 1-(chloromethyl)-2-methylbenzene (0.657 g, 4.67 mmol) was added. The mixture was heated to reflux for 3 h and then cooled to room temperature. Water (40 mL) was added to the reaction mixture and the product was extracted with DCM (3 × 40 mL). The combined organic layers were washed with brine and dried with anhydrous Na_2SO_4. The solvent was removed *in vacuo* to afford **6c** as a white solid (1.251 g, 80%). ^1H NMR (250 MHz, $CDCl_3$) δ 7.32–7.23 (m, 1H), 7.23–7.10 (m, 3H), 4.63 (s, 1H), 3.44 (s, 2H), 3.02 (app t, J = 6.4 Hz, 2H), 2.89 (app d, J = 11.7 Hz, 2H), 2.36 (s, 3H), 1.98 (app t, J = 11.5 Hz, 2H), 1.89–1.56 (m, 2H), 1.45 (s, 10H), 1.35–1.14 (m, 2H). ESI-MS m/z: 319.15 $[M + H]^+$.

4.3.2.2. General procedure B. N-Boc deprotection. A solution of HCl in dioxane (4 M) was added to a solution of *tert*-butyl ((1-benzylpiperidin-4-yl)methyl)carbamate **6** in dioxane. The reaction mixture was stirred for 1–3 h at room temperature, the completion was determined by TLC. The precipitated salt was filtered and washed with EtOAc (~5 mL). To this crude salt product, aqueous 10% K_2CO_3 solution was added to reach pH ~10–11. Extraction was performed with DCM (3x). The combined organic layers were washed with brine and dried with anhydrous Na_2SO_4. The solvent was removed *in vacuo* and to afford pure product after drying overnight *in vacuo* at 40 °C.

The compounds **2, 7b-l** were prepared from the corresponding Boc-protected amines **6a-l** following the general procedure B. Compounds **7g** and **7h** were isolated as hydrochloride salts.

*4.3.2.2.1. (1-(2-Chlorobenzyl)piperidin-4-yl)methanamine **(2)**.* The general procedure B was followed using **6a** (2.500 g, 7.38 mmol), dioxane (10 mL), HCl in dioxane (4 M, 10 mL) and a reaction time of 1 h. Compound **2** was obtained as a yellow oil (1.570 g, 89%). ^1H NMR (500 MHz, $CDCl_3$) δ 7.46 (dd, J = 1.7, 7.7 Hz, 1H), 7.31 (dd, J = 7.9, 1.4 Hz, 1H), 7.20 (td, J = 7.4, 1.3 Hz, 1H), 7.14 (td, J = 7.6, 1.8 Hz, 1H), 3.58 (s, 2H), 2.96–2.86 (m, 2H), 2.56 (d, J = 5.8 Hz, 2H), 2.05 (app t, J = 11.2 Hz, 2H), 1.75–1.63 (m, 2H), 1.31–1.19 (m, 5H). ^{13}C NMR (126 MHz, $CDCl_3$) δ 136.5, 134.2, 130.63, 129.4, 127.9, 126.6, 59.6, 53.9, 48.3, 39.4, 30.1. HR-MS m/z $[M + H]^+$ calc. for $C_{13}H_{20}ClN_2^+$ 239.1310; found 239.1319.

*4.3.2.2.2. (1-(3,4-Dichlorobenzyl)piperidin-4-yl)methanamine **(7b)**.* The general procedure B was followed using **6b** (2.500 g, 7.38 mmol), dioxane (10 mL), HCl in dioxane (4 M, 10 mL) and a reaction time of 1 h. Compound **7b** was obtained as a yellow oil (0.640 g, 88%). ^1H NMR (500 MHz, $CDCl_3$) δ 7.33 (d, J = 2.0 Hz, 1H), 7.26 (d, J = 8.2 Hz, 1H), 7.05 (dd, J = 8.2, 2.0 Hz, 1H), 3.31 (s, 2H), 2.74 (app d, J = 10.8 Hz, 2H), 2.48 (d, J = 6.1 Hz, 2H), 1.84 (app t, J = 11.4 Hz, 2H), 1.63–1.56 (m, 2H), 1.38 (s, 2H), 1.23–1.08 (m, 3H). ^{13}C NMR (126 MHz, $CDCl_3$) δ 139.2, 132.0, 130.6, 130.5, 129.9, 128.2, 62.0, 53.53, 48.0, 39.1, 29.8. HRMS-ESI m/z $[M + H]^+$ calc. for $C_{13}H_{18}Cl_2N_2^+$ 273.0920; found 273.0924.

*4.3.2.2.3. (1-(2-Methylbenzyl)piperidin-4-yl)methanamine **(7c)**.* The general procedure B was followed using **6c** (0.500 g, 1.57 mmol), dioxane (4 mL), HCl in dioxane (4 M, 4 mL) and a reaction time of 1 h. Compound **7c** was obtained as a yellow oil (0.640 g, 88%). ^1H NMR (250 MHz, $CDCl_3$) δ 7.35–7.05 (m, 4H), 3.42 (s, 2H), 2.96–2.79 (m, 2H), 2.57 (d, J = 6.0 Hz, 2H), 2.35 (s, 3H), 2.06–1.85 (m, 2H), 1.75–1.56 (m, 4H), 1.46–1.07 (m, 3H). ^{13}C NMR (63 MHz, $CDCl_3$) δ 137.5, 137.1, 130.2, 129.8, 126.9, 125.5, 61.2, 53.9,

48.2, 39.4, 30.2, 19.4. HRMS-ESI *m/z* $[M + H]^+$ calc. for $C_{14}H_{23}N_2^+$ 219.1861; found 219.1866.

*4.3.2.2.4. (1-(2-Methoxybenzyl)piperidin-4-yl)methanamine **(7d)**.* The general procedure B was followed using **6d** (2.180 g, 6.52 mmol), dioxane (10 mL), HCl in dioxane (4 M, 10 mL) and a reaction time of 3 h. Compound **7d** was obtained as a pale yellow oil (1.200 g, 79%). ^{1}H NMR (500 MHz, $CDCl_3$) δ 7.33 (d, *J* = 7.4 Hz, 1H), 7.20 (t, *J* = 8.0 Hz, 1H), 6.91 (t, *J* = 7.3 Hz, 1H), 6.83 (d, *J* = 8.2 Hz, 1H), 3.78 (s, 3H), 3.53 (s, 2H), 2.93 (app d, *J* = 10.7 Hz, 2H), 2.54 (br s, 2H), 1.99 (app t, *J* = 10.6 Hz, 2H), 1.66 (app d, *J* = 7.7 Hz, 2H), 1.35–1.17 (m, 5H). ^{13}C NMR (151 MHz, $CDCl_3$) δ 157.8, 130.5, 127.8, 126.7, 120.3, 110.4, 56.4, 55.4, 53.7, 48.26, 39.4, 30.1. HRMS-ESI *m/z* $[M + H]^+$ calc. for $C_{14}H_{23}N_2O^+$ 235.1810; found 235.1795.

*4.3.2.2.5. (1-(Cyclohexylmethyl)piperidin-4-yl)methanamine **(7e)**.* The general procedure B was followed using **6e** (0.400 g, 1.93 mmol), dioxane (3 mL), HCl in dioxane (4 M, 3 mL) and a reaction time of 1 h. Compound **7e** was obtained as a yellow oil (0.200 g, 74%). ^{1}H NMR (250 MHz, $CDCl_3$) δ 2.94 (app d, *J* = 11.5 Hz, 2H), 2.63 (d, *J* = 5.5 Hz, 2H), 2.16 (d, *J* = 7.0 Hz, 2H), 2.01–1.43 (m, 13H), 1.41–1.06 (m, 5H), 1.06–0.73 (m, 2H). ^{13}C NMR (63 MHz, $CDCl_3$) δ 66.3, 54.4, 48.3, 39.6, 35.4, 32.2, 30.1, 26.9, 26.3. HRMS-ESI *m/z* $[M + H]^+$ calc. for $C_{13}H_{27}N_2^+$ 211.2174; found 211.2178.

*4.3.2.2.6. 2-(1-(2-Chlorobenzyl)piperidin-4-yl)ethan-1-amine **(7f)**.* The general procedure B was followed using **6f** (0.330 g, 0.94 mmol), dioxane (2 mL), HCl in dioxane (4 M, 2 mL) and a reaction time of 1 h. Compound **7f** was obtained as a yellow oil (0.160 g, 67%). ^{1}H NMR (500 MHz, $CDCl_3$) δ 7.43 (dd, *J* = 7.7, 1.8 Hz, 1H), 7.28 (dd, *J* = 7.9, 1.5 Hz, 1H), 7.17 (td, *J* = 7.5, 1.5 Hz, 1H), 7.11 (td, *J* = 7.6, 1.8 Hz, 1H), 3.53 (s, 2H), 2.88–2.81 (m, 2H), 2.67 (t, *J* = 7.2 Hz, 2H), 2.00 (app t, *J* = 11.4 Hz, 2H), 1.60 (app d, *J* = 12.6 Hz, 2H), 1.38–1.19 (m, 5H), 1.12 (br s, 2H). ^{13}C NMR (126 MHz, $CDCl_3$) δ 136.4, 134.1, 130.5, 129.2, 127.8, 126.48, 59.6, 54.0, 40.7, 39.6, 33.3, 32.5. HRMS-ESI *m/z* $[M + H]^+$ calc. for $C_{14}H_{22}ClN_2^+$ 253.1466; found 253.1471.

*4.3.2.2.7. (1-Benzylpiperidin-4-yl)methanamine dihydrochloride **(7g)**.* The general procedure B was followed using **6g** (2.500 g, 8.21 mmol), dioxane (10 mL), HCl in dioxane (4 M, 15 mL) and a reaction time of 2 h. Basic extraction was omitted and compound **7g** was obtained as the dihydrochloride salt (2.260 g, 99%). Due to the proton exchange with D_2O, the ammonium groups are not visible in NMR spectra. ^{1}H NMR (500 MHz, D_2O) δ 7.55–7.34 (m, 5H), 4.26 (s, 2H), 3.60–3.40 (m, 2H), 3.11–2.84 (m, 4H), 2.11–1.86 (m, 3H), 1.59–1.32 (m, 2H). ESI-MS *m/z*: 205.10 $[M + H]^+$ (free amine).

*4.3.2.2.8. (1-Benzylpiperidin-4-yl)methanamine dihydrochloride **(7h)**.* The general procedure B was followed using **6h** (2.000 g, 6.24 mmol), dioxane (10 mL), HCl in dioxane (4 M, 10 mL) and a reaction time of 3 h. Basic extraction was omitted and compound **7h** was obtained as the dihydrochloride salt (1.770 g, 97%). Due to the proton exchange with D_2O, the OH and ammonium groups are not visible in NMR spectra. ^{1}H NMR (500 MHz, D_2O) δ 7.33 (d, *J* = 8.6 Hz, 2H), 6.92 (d, *J* = 8.5 Hz, 2H), 4.19 (s, 2H), 3.52 (app d, *J* = 12.7 Hz, 2H), 2.98 (app t, *J* = 13.0 Hz, 2H), 2.92 (d, *J* = 6.8 Hz, 2H), 2.06–1.92 (m, 3H), 1.52–1.39 (m, 2H). ESI-MS *m/z*: 221.05 $[M + H]^+$ (free amine).

*4.3.2.2.9. (1-(4-Chlorobenzyl)piperidin-4-yl)methanamine **(7i)**.* The general procedure B was followed using **6i** (0.580 g, 1.72 mmol), dioxane (8 mL), HCl in dioxane (4 M, 8 mL) and a reaction time of 3 h. Compound **7i** was obtained as a yellow oil (0.300 g, 73%). ^{1}H NMR (500 MHz, $CDCl_3$) 7.30–7.21 (m, 4H), 3.44 (s, 2H), 2.86 (app d, *J* = 11.1 Hz, 2H), 2.57 (d, *J* = 5.9 Hz, 2H), 1.93 (app t, *J* = 11.7 Hz, 2H), 1.72–1.65 (m, 2H), 1.50 (br s, 3H), 1.27–1.16 (m, 2H). ESI-MS *m/z*: 239.05 $[M + H]^+$.

*4.3.2.2.10. (1-(3-Chlorobenzyl)piperidin-4-yl)methanamine **(7j)**.* The general procedure B was followed using **6j** (0.520 g, 1.53 mmol), dioxane (5 mL), HCl in dioxane (4 M, 5 mL) and a reaction time of 3 h. Compound **7j** was obtained as a yellow oil (0.210 g, 58%). ^{1}H NMR (500 MHz, $CDCl_3$) 7.31 (s, 1H), 7.25-7.14 (m, 3H), 3.44 (s, 2H), 2.86 (app d, *J* = 11.7 Hz, 2H), 2.57 (d, *J* = 5.5 Hz, 2H), 1.93 (app t, *J* = 11.5 Hz, 2H), 1.68 (app d, *J* = 12.0 Hz, 2H), 1.46 (br s, 2H), 1.33-1.17 (m, 3H). ESI-MS *m/z*: 239.10 $[M + H]^+$.

*4.3.2.2.11. (1-(2,3-Dichlorobenzyl)piperidin-4-yl)methanamine **(7k)**.* The general procedure B was followed using **6k** (0.490 g, 1.32 mmol), dioxane (5 mL), HCl in dioxane (4 M, 5 mL) and a reaction time of 3 h. Compound **7k** was obtained as a yellow oil (0.270 g, 74%). ^{1}H NMR (500 MHz, $CDCl_3$) δ 7.41 (d, *J* = 7.2 Hz, 1H), 7.34 (dt, *J* = 1.8, 8.1 Hz, 1H), 7.16 (td, *J* = 7.0, 6.2, 1.6 Hz, 1H), 3.62–3.56 (m, 2H), 3.08 (app d, *J* = 6.7 Hz, 1H), 2.95–2.84 (m, 2H), 2.58 (d, *J* = 5.9 Hz, 1H), 2.09 (qd, *J* = 11.9, 5.8 Hz, 2H), 1.80 (app d, *J* = 7.4 Hz, 2H), 1.78–1.62 (m, 2H), 1.31–1.23 (m, 3H). ESI-MS *m/z*: 273.05 $[M + H]^+$.

*4.3.2.2.12. (1-(2,6-Dichlorobenzyl)piperidin-4-yl)methanamine **(7l)**.* The general procedure B was followed using **6l** (0.630 g, 1.70 mmol), dioxane (5 mL), HCl in dioxane (4 M, 5 mL) and a reaction time of 3 h. Compound **7l** was obtained as a yellow solid (0.340 g, 74%). ^{1}H NMR (500 MHz, $CDCl_3$) δ 7.28 (d, *J* = 8.0 Hz, 2H), 7.11 (t, *J* = 8.0 Hz, 1H), 3.70 (s, 2H), 2.92 (app d, *J* = 11.5 Hz, 2H), 2.55 (d, *J* = 6.5 Hz, 2H), 2.18 (app t, *J* = 11.6 Hz, 2H), 1.65 (app d, *J* = 13.2 Hz, 4H), 1.35–1.24 (m, 1H), 1.13–1.22 (m, 2H). ESI-MS *m/z*: 273.00 $[M + H]^+$.

4.3.2.3. General procedure C. Indirect reductive amination. Step I: To a mixture of (1-benzylpiperidin-4-yl)methanamine **2** or **7d,g-l** (typically 1.0 eq) and anhydrous Na_2SO_4 (typically 6.0 eq) in DCM (for compounds **7h** and **7g**, TEA (2.0 eq) was added), the corresponding benzaldehyde (typically 1.0 eq) was added. The mixture was stirred at rt until imine conversion was finished as judged by NMR analysis of a sample after mini-workup. The reaction mixture was filtered and the filtrate was evaporated *in vacuo* to afford the crude imine product.

Step II: The crude imine product (theoretically 1.0 eq) was dissolved in MeOH and sodium borohydride ($NaBH_4$) (typically 1.4 eq) was slowly added to the reaction mixture. The mixture was stirred at rt until conversion was finished as judged by TLC analysis (ca. 10–30 min.). The reaction mixture was quenched with water (~2 mL) and acetone (~2 mL), stirred for 10 min and concentrated under reduced pressure. 10% K_2CO_3 aqueous solution was added until pH ~10–11, and the product was extracted with DCM (3x). The combined organic layers were washed with brine (1x) and dried with anhydrous Na_2SO_4. The solvent was evaporated to give crude product **8**. In case of impurities, flash column chromatography was used for purification using cyclohexane/5%TEA: EtOAc/5%TEA and a gradient flow from 100-0% to 50-50%.

The compounds **8**–**19**, **22**–**28** and **30**–**32** were prepared from the corresponding amines following the general procedure C. Compounds **20**, **21** and **29** were obtained as fumarate salts according to the general procedure C followed by treatment with fumaric acid.

*4.3.2.3.1. N-benzyl-1-(1-benzylpiperidin-4-yl)methanamine **(8)**.* The general procedure C was followed using **7g** (0.280 g, 1.00 mmol), benzaldehyde (0.110 g, 1 mmol), TEA (0.200 g, 2.00 mmol), Na_2SO_4 (0.850 g, 6.00 mmol), DCM (10 mL) and a reaction time of 22 h. Imine reduction was performed with $NaBH_4$ (0.053 g, 1.40 mmol), MeOH (12 mL) and reaction time of 30 min. Compound **8** was obtained as pale yellow oil (0.200 g, 67%). ^{1}H NMR (500 MHz, $CDCl_3$) δ 7.35–7.28 (m, 8H), 7.26–7.22 (m, 2H), 3.77 (s, 2H), 3.49 (s, 2H), 2.89 (app d, *J* = 11.5 Hz, 2H), 2.51 (d, *J* = 6.8 Hz, 2H), 1.95 (app t, *J* = 12.6 Hz, 2H), 1.70 (app d, *J* = 13.4 Hz, 3H), 1.54–1.43 (m, 1H), 1.27 (qd, *J* = 12.3, 3.7 Hz, 2H). ^{13}C NMR (126 MHz, $CDCl_3$) δ 140.6, 138.5, 129.4, 128.5, 128.3, 128.2, 127.1, 127.0, 63.6, 55.5, 54.2, 53.8, 36.3, 30.6. HRMS-ESI *m/z* $[M + H]^+$ calc. for $C_{20}H_{27}N_2^+$ 295.2174; found 295.2155.

*4.3.2.3.2. 4-((4-((Benzylamino)methyl)piperidin-1-yl)methyl) phenol **(9)**.* The general procedure C was followed using **7h**

(0.240 g, 0.80 mmol), benzaldehyde (0.085 g, 0.80 mmol), TEA (0.162 g, 1.60 mmol), Na_2SO_4 (0.682 g, 4.80 mmol), DCM (12 mL) and a reaction time of 5 days. Imine reduction was performed with $NaBH_4$ (0.042 g, 1.12 mmol), MeOH (12 mL) and reaction time of 30 min. Compound **9** was obtained as a yellow solid (0.11 g, 46%). Mp: 83.9–93.8 °C. H NMR (500 MHz, $CDCl_3$) δ 7.39–7.22 (m, 5H), 7.06 (d, J = 8.1 Hz, 2H), 6.59 (d, J = 8.0 Hz, 2H), 3.76 (s, 2H), 3.43 (s, 2H), 3.24–2.82 (m, 4H), 2.51 (d, J = 6.5 Hz, 2H), 1.98 (app t, J = 11.0 Hz, 2H), 1.71 (app d, J = 12.2 Hz, 2H), 1.59–1.45 (m, 1H), 1.30 (qd, J = 12.1, 3.7 Hz, 2H). ^{13}C NMR (126 MHz, $CDCl_3$) δ 156.0, 140.1, 131.2, 128.6, 128.3, 128.1, 127.2, 115.6, 62.88, 55.1, 54.2, 53.3, 36.0, 30.1. HRMS-ESI m/z $[M + H]^+$ calc. for $C_{20}H_{27}N_2O^+$ 311.2123; found 325.2270.

*4.3.2.3.3. N-benzyl-1-(1-(2-methoxybenzyl)piperidin-4-yl)methanamine **(10)**.* The general procedure C was followed using **7d** (0.234 g, 1.00 mmol), benzaldehyde (0.106 g, 1.00 mmol), Na_2SO_4 (0.850 g, 6.00 mmol), DCM (12 mL) and a reaction time of 42 h. Imine reduction was performed with $NaBH_4$ (0.053 g, 1.40 mmol), MeOH (12 mL) and reaction time of 15 min. Compound **10** was obtained as a colorless oil (0.15 g, 47%).^{1}H NMR (500 MHz, $CDCl_3$) δ 7.37–7.29 (m, 5H), 7.25–7.20 (m, 2H), 6.93 (t, J = 7.4 Hz, 1H), 6.86 (d, J = 8.2 Hz, 1H), 3.81 (s, 3H), 3.77 (s, 2H), 3.54 (s, 2H), 2.94 (app d, J = 11.5 Hz, 2H), 2.51 (d, J = 6.7 Hz, 2H), 2.01 (app t, J = 11.2 Hz, 2H), 1.70 (app d, J = 12.5 Hz, 2H), 1.54–1.43 (m, 1H), 1.29 (qd, J = 12.2, 3.7 Hz, 2H). ^{13}C NMR (126 MHz, $CDCl_3$) δ 157.9, 140.7, 130.6, 128.5, 128.2, 128.0, 127.0, 126.7, 120.4, 110.5, 56.5, 55.6, 54.2, 53.8, 30.7. HRMS-ESI m/z $[M + H]^+$ calc. for $C_{21}H_{29}N_2O^+$ 325.2280; found 325.2270.

*4.3.2.3.4. 1-(1-(2-Methoxybenzyl)piperidin-4-yl)-N-(3-methylbenzyl)methanamine **(11)**.* The general procedure C was followed using **7d** (0.230 g, 1.00 mmol) and 3-methylbenzaldehyde (0.120 g, 1.00 mmol)), Na_2SO_4 (0.850 g, 6.00 mmol), DCM (12 mL) and a reaction time of 52 h. Imine reduction was performed with $NaBH_4$ (0.053 g, 1.40 mmol), MeOH (12 mL) and reaction time of 20 min. Compound **11** was obtained as a colourless oil (0.28 g, 82%).^{1}H NMR (500 MHz, $CDCl_3$) δ 7.38 (d, J = 7.3 Hz, 1H), 7.25–7.17 (m, 2H), 7.13 (s, 1H), 7.10 (d, J = 7.5 Hz, 1H), 7.06 (d, J = 7.4 Hz, 1H), 6.94 (t, J = 7.4 Hz, 1H), 6.87 (d, J = 8.2 Hz, 1H), 3.81 (s, 3H), 3.73 (s, 2H), 3.61 (s, 2H), 2.99 (app d, J = 11.2 Hz, 2H), 2.51 (d, J = 6.7 Hz, 2H), 2.34 (s, 3H), 2.08 (app t, J = 11.5 Hz, 2H), 1.72 (app d, J = 12.8 Hz, 2H), 1.56–1.45 (m, 1H), 1.42–1.30 (m, 2H). ^{13}C NMR (126 MHz, $CDCl_3$) δ 157.9, 140.1, 138.1, 130.9, 129.0, 128.4, 128.2, 127.8, 125.8, 125.2, 120.4, 110.5, 56.2, 55.5, 55.3, 54.1, 53.5, 35.9, 30.4, 21.5. HRMS-ESI m/z $[M + H]^+$ calc. for $C_{22}H_{31}N_2O^+$ 339.2436; found 339.2422.

*4.3.2.3.5. N-(3-ethylbenzyl)-1-(1-(2-methoxybenzyl)piperidin-4-yl)methanamine **(12)**.* The general procedure C was followed using **7d** (0.120 g, 0.50 mmol) and 3-ethylbenzaldehyde (0.067 g, 0.50 mmol), Na_2SO_4 (0.426 g, 3.00 mmol), DCM (8 mL) and a reaction time of 4 days. Imine reduction was performed with $NaBH_4$ (0.026 g, 0.70 mmol), MeOH (8 mL) and reaction time of 30 min. Compound **12** was obtained as a colorless oil (0.093 g, 53%). ^{1}H NMR (500 MHz, $CDCl_3$) δ 7.37 (d, J = 7.2 Hz, 1H), 7.25–7.20 (m, 2H), 7.15 (s, 1H), 7.10 (dd, J = 17.8, 7.6 Hz, 2H), 6.94 (t, J = 7.4 Hz, 1H), 6.86 (d, J = 8.1 Hz, 1H), 3.82 (s, 3H), 3.75 (s, 2H), 3.57 (s, 2H), 2.96 (app d, J = 12.0 Hz, 2H), 2.64 (q, J = 7.6 Hz, 2H), 2.53 (d, J = 6.7 Hz, 2H), 2.04 (app t, J = 11.3 Hz, 2H), 1.71 (app d, J = 12.4 Hz, 2H), 1.56–1.45 (m, 1H), 1.32 (qd, J = 12.2 3.7 Hz, 2H), 1.24 (t, J = 7.6 Hz, 3H). ^{13}C NMR (126 MHz, $CDCl_3$) δ 157.9, 144.5, 140.5, 130.8, 128.4, 128.1, 127.7, 126.5, 126.3, 125.5, 120.4, 110.5, 56.4, 55.6, 55.5, 54.3, 53.7, 36.1, 30.6, 28.9, 15.8. HRMS-ESI m/z $[M + H]^+$ calc. for $C_{22}H_{33}N_2O^+$ 353.2593; found 353.2586.

*4.3.2.3.6. N-benzyl-1-(1-(2-chlorobenzyl)piperidin-4-yl)methanamine **(13)**.* The general procedure C was followed using **2** (0.210 g, 0.87 mmol) and benzaldehyde (0.089 g, 0.83 mmol), Na_2SO_4 (0.710 g, 5.00 mmol), DCM (10 mL) and a reaction time of 27 h. Imine reduction was performed with $NaBH_4$ (0.047 g, 1.24 mmol), MeOH (10 mL) and reaction time of 30 min. Compound **13** was obtained as a yellow oil (0.20 g, 75%). ^{1}H NMR (500 MHz, $CDCl_3$) δ 7.46-7.40 (m, 1H), 7.33–7.23 (m, 5H), 7.22–7.14 (m, 2H), 7.13-7.08 (m, 1H), 3.73 (s, 2H), 3.54 (s, 2H), 2.85 (app d, J = 11.6 Hz, 2H), 2.47 (d, J = 6.8 Hz, 2H), 2.01 (app t, J = 11.7 Hz, 2H), 1.66 (app d, J = 12.5 Hz, 2H), 1.56–1.39 (m, 2H), 1.29–1.18 (m, 2H). ^{13}C NMR (126 MHz, $CDCl_3$) δ 140.6, 136.5, 134.2, 130.7, 129.4, 128.5, 128.1, 127.9, 127.0, 126.6, 59.67, 55.5, 54.2, 53.9, 36.2, 30.8. HRMS-ESI m/z $[M + H]^+$ calc. for $C_{20}H_{26}ClN_2^+$ 329.1779; found 329.1788.

*4.3.2.3.7. 1-(1-(2-Chlorobenzyl)piperidin-4-yl)-N-(pyridin-3-ylmethyl)methanamine **(14)**.* The general procedure C was followed using **2** (0.210 g, 0.87 mmol) and nicotinaldehyde (0.091 g, 0.83 mmol), Na_2SO_4 (0.71 g, 5.00 mmol), DCM (10 mL) and a reaction time of 24 h. Imine reduction was performed with $NaBH_4$ (0.047 g, 1.24 mmol), MeOH (10 mL) and reaction time of 30 min. Compound **14** was obtained as a yellow oil (0.200 g, 73%). ^{1}H NMR (500 MHz, $CDCl_3$) δ 8.55 (d, J = 2.1 Hz, 1H), 8.49 (dd, J = 1.7, 4.8 Hz, 1H), 7.67 (dt, J = 2.0, 7.8 Hz, 1H), 7.48 (d, J = 7.9 Hz, 1H), 7.33 (dd, J = 7.9, 1.4 Hz, 1H), 7.25–7.20 (m, 2H), 7.16 (td, J = 7.6, 1.8 Hz, 1H), 3.79 (s, 2H), 3.60 (s, 2H), 2.91 (app d, J = 11.5 Hz, 2H), 2.51 (d, J = 6.7 Hz, 2H), 2.08 (app t, J = 11.6 Hz, 2H), 1.77–1.67 (m, 2H), 1.58–1.40 (m, 2H), 1.29 (app q, J = 12.0 Hz, 2H). ^{13}C NMR (126 MHz, $CDCl_3$) δ 149.8, 148.6, 136.4, 136.0, 135.8, 134.3, 130.8, 129.4, 128.1, 126.7, 123.5, 59.6, 55.5, 53.9, 51.6, 36.3, 30.7. HRMS-ESI m/z $[M + H]^+$ calc. for $C_{19}H_{25}ClN_3^+$ 330.1732; found 330.1716.

*4.3.2.3.8. N-((1H-Imidazol-4-yl)methyl)-1-(1-(2-chlorobenzyl)piperidin-4-yl)methanamine **(15)**.* The general procedure C was followed using **2** (0.240 g, 0.97 mmol) and 1*H*-imidazole-4-carbaldehyde (0.091 g, 0.93 mmol), Na_2SO_4 (0.790 g, 5.56 mmol), DCM (10 mL) and a reaction time of 24 h. Imine reduction was performed with $NaBH_4$ (0.053 g, 1.40 mmol), MeOH (12 mL) and reaction time of 30 min. Compound **15** was obtained as a yellow oil (0.290 g, 96%). ^{1}H NMR (500 MHz, CD_3OD) δ 7.66 (d, J = 1.2 Hz, 1H), 7.47 (dd, J = 7.5, 2.0 Hz, 1H), 7.37 (dd, J = 7.7, 1.6 Hz, 1H), 7.30–7.22 (m, 2H), 7.04 (s, 1H), 3.79 (s, 2H), 3.63 (s, 2H), 2.94 (app d, J = 12.1 Hz, 2H), 2.55 (d, J = 6.8 Hz, 2H), 2.12 (app t, J = 11.8 Hz, 2H), 1.78–1.68 (m, 2H), 1.62–1.53 (m, 1H), 1.31–1.21 (m, 2H). ^{13}C NMR (126 MHz, CD_3OD) δ 136.6, 136.5, 135.7, 132.6, 130.5, 129.7, 127.9, 60.3, 55.3, 54.5, 46.2, 36.3, 31.1. The ^{13}C NMR spectrum has two missing peaks. A 2D-NMR spectrum was recorded to prove the structure and one missing peak was identified by HSQC (Fig. S7). HRMS-ESI m/z $[M + H]^+$ calc. for $C_{17}H_{24}ClN_4^+$ 319.1684; found 319.1685.

*4.3.2.3.9. 1-(1-(2-Chlorobenzyl)piperidin-4-yl)-N-(cyclohexylmethyl)methanamine **(16)**.* The general procedure C was followed using **2** (0.180 g, 0.75 mmol) and cyclohexanecarbaldehyde (0.084 g, 0.75 mmol), Na_2SO_4 (0.639 g, 4.50 mmol), DCM (12 mL) and a reaction time of 41 h. Imine reduction was performed with $NaBH_4$ (0.040 g, 1.05 mmol), MeOH (12 mL) and reaction time of 30 min. Compound **16** was obtained as a yellow oil (0.210 g, 84%). ^{1}H NMR (500 MHz, $CDCl_3$) δ 7.46 (d, J = 7.6 Hz, 1H), 7.32 (d, J = 7.8 Hz, 1H), 7.22 (t, J = 7.5 Hz, 1H), 7.16 (t, J = 7.6 Hz, 1H), 3.58 (s, 2H), 2.90 (app d, J = 11.2 Hz, 2H), 2.47 (d, J = 6.8 Hz, 2H), 2.42 (d, J = 6.7 Hz, 2H), 2.05 (app t, J = 11.4 Hz, 2H), 1.83–1.57 (m, 7H), 1.56–1.36 (m, 2H), 1.36–1.05 (m, 5H), 0.94–0.80 (m, 2H). ^{13}C NMR (126 MHz, $CDCl_3$) δ 136.5, 134.3, 130.7, 129.4, 128.0, 126.6, 59.7, 56.8, 56.0, 53.9, 37.7, 35.9, 31.5, 30.8, 26.8, 26.1. HRMS-ESI m/z $[M + H]^+$ calc. for $C_{20}H_{32}ClN_2^+$ 335.2254; found 335.2239.

*4.3.2.3.10. 1-(1-(2-Chlorobenzyl)piperidin-4-yl)-N-(2,3-dichlorobenzyl)methanamine **(17)**.* The general procedure C was followed using **2** (0.143 g, 0.60 mmol) and 2,3-dichlorobenzaldehyde (0.110 g, 0.60 mmol), Na_2SO_4 (0.511 g, 3.60 mmol), DCM (10 mL) and a reaction time of 22 h. Imine reduction was performed with $NaBH_4$ (0.032 g, 0.84 mmol), MeOH (10 mL) and reaction time of 30 min.

Compound **17** was obtained as a yellow oil (0.175 g, 73%). ^{1}H NMR (500 MHz, $CDCl_3$) δ 7.47 (d, J = 7.7 Hz, 1H), 7.36 (d, J = 8.0 Hz, 1H), 7.35–7.28 (m, 2H), 7.25–7.14 (m, 3H), 3.89 (s, 2H), 3.59 (s, 2H), 2.91 (app d, J = 10.7 Hz, 2H), 2.50 (d, J = 6.1 Hz, 2H), 2.07 (app t, J = 11.5 Hz, 2H), 1.72 (app d, J = 12.6 Hz, 2H), 1.67–1.34 (m, 2H), 1.29 (app q, J = 12.1 Hz, 2H). ^{13}C NMR (151 MHz, $CDCl_3$) δ 140.4, 136.6, 134.3, 133.2, 131.9, 130.7, 129.4, 129.1, 128.1, 128.0, 127.3, 126.7, 59.7, 55.4, 53.9, 52.2, 36.3, 30.8. HRMS-ESI m/z $[M + H]^+$ calc. for $C_{20}H_{24}Cl_3N_2^+$ 397.1005; found 397.0987.

4.3.2.3.11. 1-(1-(2-Chlorobenzyl)piperidin-4-yl)-N-(4-methoxybenzyl)methanamine ***(18)***. The general procedure C was followed using **2** (0.160 g, 0.65 mmol) and 4-methoxybenzaldehyde (0.088 g, 0.65 mmol), Na_2SO_4 (0.554 g, 3.90 mmol), DCM (10 mL) and a reaction time of 45 h. Imine reduction was performed with $NaBH_4$ (0.034 g, 0.91 mmol), MeOH (10 mL) and reaction time of 30 min Compound **18** was obtained as a yellow oil (0.175 g, 75%). ^{1}H NMR (500 MHz, $CDCl_3$) δ 7.47 (dd, J = 7.6, 1.7 Hz, 1H), 7.33 (dd, J = 7.9, 1.3 Hz, 1H), 7.25–7.20 (m, 3H), 7.16 (td, J = 7.6, 1.8 Hz, 1H), 6.91–6.81 (m, 2H), 3.79 (s, 3H), 3.72 (s, 2H), 3.59 (s, 2H), 2.91 (app d, J = 11.8 Hz, 2H), 2.51 (d, J = 6.7 Hz, 2H), 2.11–1.95 (m, 3H), 1.71 (app d, J = 12.4 Hz, 2H), 1.57–1.45 (m, 1H), 1.28 (qd, J = 12.1, 3.8 Hz, 2H). ^{13}C NMR (126 MHz, $CDCl_3$)) δ 158.7, 136.4, 134.2, 132.4, 130.7, 129.4, 129.4, 128.0, 126.6, 113.8, 59.6, 55.3, 55.2, 53.8, 53.5, 36.1, 30.7. HRMS-ESI m/z $[M + H]^+$ calc. for $C_{21}H_{28}ClN_2O^+$ 359.1890; found 359.1876.

4.3.2.3.12. 1-(Benzo[d][1,3]dioxol-5-yl)-N-((1-(2-chlorobenzyl) piperidin-4-yl)methyl)methanamine ***(19)***. The general procedure C was followed using **2** (0.200 g, 0.83 mmol) and benzo[*d*] [1,3] dioxole-5-carbaldehyde (0.120 g, 0.79 mmol), Na_2SO_4 (0.67 g, 4.72 mmol), DCM (10 mL) and a reaction time of 52 h. Imine reduction was performed with $NaBH_4$ (0.045 g, 1.19 mmol), MeOH (10 mL) and reaction time of 30 min. Compound **19** was obtained as a yellow oil (0.250 g, 84%). ^{1}H NMR (500 MHz, $CDCl_3$) δ 7.47 (dd, J = 7.6, 1.7 Hz, 1H), 7.33 (dd, J = 7.8, 1.3 Hz, 1H), 7.22 (td, J = 7.5, 1.4 Hz, 1H), 7.16 (td, J = 7.6, 1.8 Hz, 1H), 6.83 (d, J = 1.2 Hz, 1H), 6.75 (d, J = 1.0 Hz, 2H), 5.93 (s, 2H), 3.68 (s, 2H), 3.59 (s, 2H), 2.91 (app d, J = 11.9 Hz, 2H), 2.49 (d, J = 6.7 Hz, 2H), 2.06 (app t, J = 11.7 Hz, 2H), 1.75–1.66 (m, 2H), 1.54–1.44 (m, 2H), 1.32–1.23 (m, 2H). ^{13}C NMR (126 MHz, $CDCl_3$) δ 147.8, 146.5, 136.6, 134.7, 134.3, 130.7, 129.4, 128.0, 126.7, 121.2, 108.7, 108.2, 101.0, 59.7, 55.3, 54.0, 53.9, 36.3, 30.8. HRMS-ESI m/z $[M + H]^+$ calc. for $C_{21}H_{26}ClN_2O_2^+$ 373.1677; found 373.1670.

4.3.2.3.13. 4-((((1-(2-Chlorobenzyl)piperidin-4-yl)methyl)amino) methyl)phenol ***(20)***. The general procedure C was followed using **2** (0.160 g, 0.65 mmol) and 4-hydroxybenzaldehyde (0.079 g, 0.65 mmol), Na_2SO_4 (0.554 g, 3.90 mmol), DCM (10 mL) and a reaction time of 44 h. Imine reduction was performed with $NaBH_4$ (0.034 g, 0.91 mmol), MeOH (10 mL) and reaction time of 30 min. Compound **20** was obtained as a white solid (0.204 g, 91%). Mp: 89.7–94.7 °C. ^{1}H NMR (500 MHz, $CDCl_3$) δ 7.46 (d, J = 7.5 Hz, 1H), 7.33 (d, J = 7.8 Hz, 1H), 7.24–7.14 (m, 2H), 7.09 (d, J = 8.1 Hz, 2H), 6.63 (d, J = 7.4 Hz, 2H), 3.68 (s, 2H), 3.60 (s, 2H), 2.92 (app d, J = 11.5 Hz, 2H), 2.65–2.34 (m, 4H), 2.07 (app t, J = 10.8 Hz, 2H), 1.70 (app d, J = 12.2 Hz, 2H), 1.63–1.48 (m, 1H), 1.27 (qd, J = 12.2, 3.9 Hz, 2H). ^{13}C NMR (126 MHz, $CDCl_3$) δ 155.5, 136.1, 134.4, 131.1, 131.0, 129.7, 129.5, 128.2, 126.7, 115.7, 59.6, 55.2, 53.8, 53.6, 35.8, 30.6. HRMS-ESI m/z $[M + H]^+$ calc. for $C_{20}H_{26}ClN_2O^+$ 345.1734; found 345.1721.

4.3.2.3.14. N-(4-chlorobenzyl)-1-(1-(2-chlorobenzyl)piperidin-4-yl)methanamine ***(23)***. The general procedure C was followed using **2** (0.167 g, 0.70 mmol) and 4-chlorobenzaldehyde (0.098 g, 0.70 mmol), Na_2SO_4 (0.597 g, 4.20 mmol), DCM (12 mL) and a reaction time of 29 h. Imine reduction was performed with $NaBH_4$ (0.037 g, 0.98 mmol), MeOH (12 mL) and reaction time of 30 min. Compound **23** was obtained as a yellow oil (0.185 g, 73%). ^{1}H NMR (500 MHz, $CDCl_3$) δ 7.47 (d, J = 7.5 Hz, 1H), 7.33 (d, J = 7.8 Hz, 1H), 7.31–7.20 (m, 5H), 7.17 (t, J = 7.6 Hz, 1H), 3.74 (s, 2H), 3.59 (s, 2H), 2.91 (app d, J = 11.0 Hz, 2H), 2.49 (d, J = 6.6 Hz, 2H), 2.06 (app t, J = 11.7 Hz, 2H), 1.71 (app d, J = 12.5 Hz, and br s, 3H, overlapping), 1.55–1.42 (m, 1H), 1.27 (qd, J = 12.2, 3.7 Hz, 2H). ^{13}C NMR (126 MHz, $CDCl_3$) δ 138.9, 136.4, 134.3, 130.8, 129.5, 129.4, 128.6, 128.1, 126.7, 59.6, 55.3, 53.9, 53.4, 36.2, 30.7. HRMS-ESI m/z $[M + H]^+$ calc. for $C_{20}H_{25}Cl_2N_2^+$ 363.1395; found 363.1383.

4.3.2.3.15. 1-(1-(2-Chlorobenzyl)piperidin-4-yl)-N-(4-methylbenzyl)methanamine ***(24)***. The general procedure C was followed using **2** (0.155 g, 0.65 mmol) and 4-methylbenzaldehyde (0.078 g, 0.65 mmol), Na_2SO_4 (0.554 g, 3.90 mmol), DCM (12 mL) and a reaction time of 65 h. Imine reduction was performed with $NaBH_4$ (0.034 g, 0.91 mmol), MeOH (12 mL) and reaction time of 25 min. Compound **24** was obtained as a yellow oil (0.150 g, 67%). ^{1}H NMR (500 MHz, $CDCl_3$) δ 7.48 (d, J = 7.2 Hz, 1H), 7.34 (d, J = 7.8 Hz, 1H), 7.25–7.12 (m, 6H), 3.76 (s, 2H), 3.59 (s, 2H), 2.92 (app d, J = 11.6 Hz, 2H), 2.52 (d, J = 6.7 Hz, 2H), 2.34 (s, 3H), 2.06 (app t, J = 11.3 Hz, and br s, 3H), 1.72 (app d, J = 12.5 Hz, 2H), 1.59–1.47 (m, 1H), 1.28 (qd, J = 12.2, 3.8 Hz, 2H). ^{13}C NMR (126 MHz, $CDCl_3$) δ 137.0, 136.6, 136.5, 134.2, 130.7, 129.4, 129.2, 128.2, 128.0, 126.6, 59.6, 55.2, 53.8, 53.8, 36.0, 30.7, 21.2. HRMS-ESI m/z $[M + H]^+$ calc. for $C_{21}H_{28}ClN_2^+$ 343.1941; found 343.1923.

4.3.2.3.16. N-(2-chlorobenzyl)-1-(1-(2-chlorobenzyl)piperidin-4-yl)methanamine ***(25)***. The general procedure C was followed using **2** (0.203 g, 0.85 mmol) and 2-chlorobenzaldehyde (0.119 g, 0.85 mmol), Na_2SO_4 (0.724 g, 5.10 mmol), DCM (12 mL) and a reaction time of 25 h. Imine reduction was performed with $NaBH_4$ (0.045 g, 1.19 mmol), MeOH (12 mL) and reaction time of 30 min. Compound **25** was obtained as a yellow oil (0.235 g, 76%). ^{1}H NMR (500 MHz, $CDCl_3$) δ 7.48 (d, J = 7.6 Hz, 1H), 7.38 (dd, J = 7.4, 1.8 Hz, 1H), 7.34 (t, J = 8.1 Hz, 2H), 7.25–7.14 (m, 4H), 3.87 (s, 2H), 3.59 (s, 2H), 2.91 (app d, J = 11.1 Hz, 2H), 2.51 (d, J = 6.4 Hz, 2H), 2.07 (app t, J = 11.8, 2.5 Hz, 2H), 1.77–1.68 (m, 2H), 1.61 (s, 1H), 1.56–1.45 (m, 1H), 1.31–1.22 (m, 2H). ^{13}C NMR (126 MHz, $CDCl_3$) δ 137.7, 134.3, 133.9, 133.8, 130.8, 130.3, 129.6, 129.4, 128.4, 128.1, 126.9, 126.7, 59.6, 55.3, 53.9, 51.7, 36.2 30.7. HRMS-ESI m/z $[M + H]^+$ calc. for $C_{20}H_{25}Cl_2N_2^+$ 363.1395; found 363.1374.

4.3.2.3.17. 1-(1-(2-Chlorobenzyl)piperidin-4-yl)-N-(2-methylbenzyl)methanamine ***(26)***. The general procedure C was followed using **2** (0.167 g, 0.70 mmol) and 2-methylbenzaldehyde (0.084 g, 0.70 mmol), Na_2SO_4 (0.597 g, 4.20 mmol), DCM (12 mL) and a reaction time of 65 h. Imine reduction was performed with $NaBH_4$ (0.037 g, 0.98 mmol), MeOH (12 mL) and reaction time of 30 min. Compound **26** was obtained as a yellow oil (0.206 g, 86%). ^{1}H NMR (500 MHz, $CDCl_3$) δ 7.49 (d, J = 7.5 Hz, 1H), 7.34 (d, J = 7.8 Hz, 1H), 7.32–7.27 (m, 1H), 7.24 (t, J = 7.5 Hz, 1H), 7.21–7.12 (m, 4H), 3.76 (s, 2H), 3.60 (s, 2H), 2.93 (app d, J = 11.4 Hz, 2H), 2.57 (d, J = 6.6 Hz, 2H), 2.35 (s, 3H), 2.08 (app t, J = 11.8 Hz, 2H), 1.74 (app d, J = 10.4 Hz, 2H), 1.64–1.40 (m, 2H), 1.30 (app q, J = 12.3 Hz, 2H). ^{13}C NMR (126 MHz, $CDCl_3$) δ 138.4, 136.4, 136.4, 134.3, 130.7, 130.4, 129.4, 128.3, 128.0, 127.0, 126.7, 126.0, 59.7, 55.9, 53.9, 51.9, 36.2, 30.8, 19.1. HRMS-ESI m/z $[M + H]^+$ calc. for $C_{21}H_{28}ClN_2^+$ 343.1941; found 343.1930.

4.3.2.3.18. 1-(1-(2-Chlorobenzyl)piperidin-4-yl)-N-(3-methylbenzyl)methanamine ***(28)***. The general procedure C was followed using **2** (0.179 g, 0.75 mmol) and 3-methylbenzaldehyde (0.090 g, 0.75 mmol), Na_2SO_4 (0.639 g, 4.50 mmol), DCM (12 mL) and a reaction time of 41 h. Imine reduction was performed with $NaBH_4$ (0.040 g, 1.05 mmol), MeOH (12 mL) and reaction time of 30 min. Compound **28** was obtained as a yellow oil (0.212 g, 82%). ^{1}H NMR (500 MHz, $CDCl_3$) δ 7.48 (d, J = 7.5 Hz, 1H), 7.34 (d, J = 7.9 Hz, 1H), 7.27–7.20 (m, 2H), 7.20–7.10 (m, 3H), 7.08 (d, J = 7.5 Hz, 1H), 3.76 (s, 2H), 3.60 (s, 2H), 2.92 (app d, J = 11.1 Hz, 2H), 2.53 (d, J = 6.6 Hz, 2H), 2.36 (s, 3H), 2.07 (app t, J = 11.7 Hz, 2H), 1.92 (br s,

1H), 1.73 (app d, J = 12.5 Hz, 2H), 1.61–1.46 (m, 1H), 1.29 (qd, J = 12.3, 3.8 Hz, 2H). ^{13}C NMR (126 MHz, $CDCl_3$) δ 140.2, 138.1, 136.4, 134.2, 130.7, 129.4, 129.00, 128.4, 128.0, 127.8, 126.6, 125.2, 59.6, 55.4, 54.1, 53.9, 36.1, 30.7, 21.5. HRMS-ESI m/z $[M + H]^+$ calc. for $C_{21}H_{28}ClN_2^+$ 343.1941; found 343.1929.

4.3.2.3.19. 1-(1-(3-Chlorobenzyl)piperidin-4-yl)-N-(3-methylbenzyl)methanamine ***(29)***. The general procedure C was followed using **7j** (0.119 g, 0.50 mmol) and 3-methylbenzaldehyde (0.060 g, 0.83 mmol), Na_2SO_4 (0.426 g, 3.00 mmol), DCM (10 mL) and a reaction time of 47 h. Imine reduction was performed with $NaBH_4$ (0.026 g, 0.70 mmol), MeOH (7 mL) and reaction time of 30 min. Compound **29** was obtained as a yellow oil (0.115 g, 67%). ^{1}H NMR (500 MHz, $CDCl_3$) δ 7.32 (s, 1H), 7.25–7.16 (m, 4H), 7.13 (s, 1H), 7.11 (d, J = 7.6 Hz, 1H), 7.06 (d, J = 7.5 Hz, 1H), 3.74 (s, 2H), 3.44 (s, 2H), 2.86 (app d, J = 11.4 Hz, 2H), 2.52 (d, J = 6.7 Hz, 2H), 2.34 (s, 3H), 1.95 (app t, J = 10.9 Hz, 2H), 1.71 (app d, J = 12.5 Hz, 2H), 1.60 (s, 1H), 1.55–1.45 (m, 1H), 1.26 (qd, J = 12.2, 3.9 Hz, 2H). ^{13}C NMR (126 MHz, $CDCl_3$) δ 141.0, 140.0, 138.2, 134.2, 129.5, 129.15, 129.0, 128.4, 127.9, 127.3, 127.2, 125.3, 63.0, 55.3, 54.1, 53.8, 36.1, 30.7, 21.5. HRMS-ESI m/z $[M + H]^+$ calc. for $C_{21}H_{28}ClN_2^+$ 343.1941; found 343.1938.

4.3.2.3.20. 1-(1-(4-Chlorobenzyl)piperidin-4-yl)-N-(3-methylbenzyl)methanamine ***(30)***. The general procedure C was followed using **7i** (0.119 g, 0.50 mmol) and 3-methylbenzaldehyde (0.060 g, 0.83 mmol), Na_2SO_4 (0.426 g, 3.00 mmol), DCM (10 mL) and a reaction time of 3 days. Imine reduction was performed with $NaBH_4$ (0.026 g, 0.70 mmol), MeOH (7 mL) and reaction time of 15 min. Compound **30** was obtained as a yellow oil (0.141 g, 82%). ^{1}H NMR (500 MHz, $CDCl_3$) δ 7.33–7.23 (m, 4H), 7.21 (d, J = 7.5 Hz, 1H), 7.14 (s, 1H), 7.11 (d, J = 7.7 Hz, 1H), 7.07 (d, J = 7.6 Hz, 1H), 3.75 (s, 2H), 3.44 (s, 2H), 2.86 (app d, J = 11.1 Hz, 2H), 2.52 (d, J = 6.7 Hz, 2H), 2.35 (s, 3H), 1.94 (app t, J = 11.6 Hz, 2H), 1.71 (d, J = 12.6 Hz, 2H), 1.57–1.39 (m, 2H), 1.31–1.21 (m, 2H). ^{13}C NMR (126 MHz, $CDCl_3$) δ 140.5, 138.1, 137.3, 132.6, 130.5, 128.9, 128.4, 127.7, 125.2, 62.8, 55.6, 54.3, 53.8, 36.3, 30.7, 21.5. HRMS-ESI m/z $[M + H]^+$ calc. for $C_{21}H_{28}ClN_2^+$ 343.1941; found 343.1920.

4.3.2.3.21. 1-(1-(2,3-Dichlorobenzyl)piperidin-4-yl)-N-(3-methylbenzyl)methanamine ***(31)***. The general procedure C was followed using **7k** (0.137 g, 0.50 mmol) and 3-methylbenzaldehyde (0.060 g, 0.50 mmol), Na_2SO_4 (0.426 g, 3.00 mmol), DCM (10 mL) and a reaction time of 3 days. Imine reduction was performed with $NaBH_4$ (0.026 g, 0.70 mmol), MeOH (7 mL) and reaction time of 15 min. Compound **31** was obtained as a yellow oil (0.128 g, 68%). ^{1}H NMR (500 MHz, $CDCl_3$) δ 7.41 (d, J = 7.7 Hz, 1H), 7.34 (d, J = 8.0 Hz, 1H), 7.21 (t, J = 7.5 Hz, 1H), 7.17 (t, J = 7.8 Hz, 1H), 7.13 (s, 1H), 7.10 (d, J = 7.6 Hz, 1H), 7.06 (d, J = 7.6 Hz, 1H), 3.74 (s, 2H), 3.60 (s, 2H), 2.89 (app d, J = 11.7 Hz, 2H), 2.52 (d, J = 6.6 Hz, 2H), 2.35 (s, 3H), 2.08 (app t, J = 11.6 Hz, 2H), 1.72 (app d, J = 12.5 Hz, 2H), 1.59–1.40 (m, 2H), 1.28 (qd, J = 12.2, 3.9 Hz, 2H). ^{13}C NMR (126 MHz, $CDCl_3$) δ 140.5, 139.2, 138.1, 133.00, 132.3, 129.00, 128.7, 128.5, 128.41, 127.8, 127.0, 125.2, 60.4, 55.6, 54.3, 54.0, 36.2, 30.80, 21.6. HRMS-ESI m/z $[M + H]^+$ calc. for $C_{21}H_{27}Cl_2N_2^+$ 377.1551; found 377.1540.

4.3.2.3.22. (1-(2,3-Dichlorobenzyl)piperidin-4-yl)methanamine ***(32)***. The general procedure C was followed using **7l** (0.123 g, 0.45 mmol) and 3-methylbenzaldehyde (0.054 g, 0.45 mmol), Na_2SO_4 (0.384 g, 2.70 mmol), DCM (10 mL) and a reaction time of 27 h. Imine reduction was performed with $NaBH_4$ (0.024 g, 0.63 mmol), MeOH (7 mL) and reaction time of 15 min. Compound **32** was obtained as a yellow oil (0.100 g, 59%). ^{1}H NMR (500 MHz, $CDCl_3$) δ 7.28 (d, J = 8.0 Hz, 2H), 7.20 (t, J = 7.5 Hz, 1H), 7.14–7.11 (m, 2H), 7.09 (d, J = 7.3 Hz, 1H), 7.05 (d, J = 7.6 Hz, 1H), 3.73 (s, 2H), 3.70 (s, 2H), 2.91 (app d, J = 11.3 Hz, 2H), 2.48 (d, J = 6.8 Hz, 2H), 2.34 (s, 3H), 2.18 (app t, J = 11.6 Hz, 2H), 1.73–1.64 (m, 3H), 1.56–1.44 (m, 1H), 1.20 (qd, J = 12.2, 3.9 Hz, 2H). ^{13}C NMR (126 MHz, $CDCl_3$) δ 140.4, 138.1, 137.1, 135.0, 129.0, 128.7, 128.4, 128.4, 127.8, 125.2, 57.0, 55.5, 54.2, 53.8, 36.1, 30.7, 21.5. HRMS-ESI m/z $[M + H]^+$ calc. for $C_{21}H_{27}Cl_2N_2^+$ 377.1551; found 377.1537.

4.3.2.3.23. 1-(1-(2-Chlorobenzyl)piperidin-4-yl)-N-(naphthalen-2-ylmethyl)methanamine fumarate ***(21)***. The general procedure C was followed using **2** (0.119 g, 0.50 mmol) and 1-naphtaldehyde (0.078 g, 0.50 mmol), Na_2SO_4 (0.426 g, 3.00 mmol), DCM (12 mL) and a reaction time of 3 days. Imine reduction was performed with $NaBH_4$ (0.027 g, 0.70 mmol), MeOH (12 mL) and reaction time of 20 min, furnishing crude 1-(1-(2-chlorobenzyl)piperidin-4-yl)-N-(naphthalen-2-ylmethyl)methanamine (free amine) containing 1-naphtaldehyde impurity as determined by NMR and HPLC. To a solution of this crude product (0.124 g, 93% pure) in 2-PrOH (10 mL), a solution of fumaric acid (0.076 g, 0.65 mmol, theoretically 2.0 eq) in 2-PrOH (5 mL) was added. The mixture was stirred at rt for 1 h. Next, the mixture was cooled in an ice bath for 1 h. The precipitate formed was filtered, washed with excess of EtOAc and extensively dried overnight in a vacuum oven at 40 °C. This afforded salt **21** as a white solid (0.153 g, overall yield 52%), which contains 1.785 eq fumarate as a salt and is a 2-PrOH solvate (0.1 eq) as determined by NMR analysis. Mp: 202.5–206.9 °C. ^{1}H NMR (500 MHz, DMSO-d_6) δ 7.91 (tt, J = 9.2, 3.9 Hz, 4H), 7.60–7.55 (m, 1H), 7.56–7.49 (m, 2H), 7.46 (dd, J = 7.6, 1.8 Hz, 1H), 7.41 (dd, J = 7.8, 1.5 Hz, 1H), 7.31 (td, J = 7.5, 1.5 Hz, 1H), 7.27 (td, J = 7.6, 1.9 Hz, 1H), 6.56 (s, 3.57H (fumarate)), 4.09 (d, J = 9.3 Hz, 2H), 3.52 (s, 2H), 2.81 (app d, J = 11.8 Hz, 2H), 2.67–2.60 (m, 2H), 2.00 (app t, J = 11.7, 2.4 Hz, 2H), 1.72 (app d, J = 12.4 Hz, 2H), 1.59 (s, 1H), 1.17 (qd, J = 12.2, 3.8 Hz, 2H). ^{13}C NMR (126 MHz, DMSO-d_6) δ 167.1, 135.7, 134.7, 133.3, 132.7, 132.6, 131.1, 130.8, 129.3, 129.0, 128.6, 128.1, 127.8, 127.7, 127.2, 127.0, 126.6, 58.8, 52.7, 51.9, 50.8, 33.1, 29.5. HRMS-ESI m/z $[M + H]^+$ calc. for $C_{24}H_{28}ClN_2^+$ 379.1941; found 379.1937.

4.3.2.3.24. 1-([1,1′-biphenyl]-3-yl)-N-((1-(2-chlorobenzyl)piperidin-4-yl)methyl)methanamine fumarate ***(22)***. The general procedure C was followed using **2** (0.119 g, 0.50 mmol), [1,1′-biphenyl]-3-carbaldehyde (0.091 g, 0.50 mmol), Na_2SO_4 (0.426 g, 3.00 mmol), DCM (12 mL) and a reaction time of 50 h. Imine reduction was performed with $NaBH_4$ (0.027 g, 0.70 mmol), MeOH (12 mL) and reaction time of 20 min, furnishing crude 1-([1,1′-biphenyl]-3-yl)-N-((1-(2-chlorobenzyl)piperidin-4-yl)methyl)methanamine (0.155 g, 90% pure). Compound **22** was prepared as described for compound **21** using corresponding crude amine (0.122 g) in 2-PrOH (10 mL), a solution of fumaric acid (0.070 g, 0.60 mmol, theoretically 2.0 eq) in 2-PrOH (5 mL) and salt formation time 3 h. Compound **22** was obtained as a white solid (0.147 g, overall yield 47%), containing 1.850 eq fumarate as a salt and is a 2-PrOH solvate (0.08 eq) as determined by NMR analysis. Mp: 189.9–193.4 °C. ^{1}H NMR (500 MHz, DMSO-d_6) δ 7.78 (br s, 1H), 7.69–7.65 (m, 2H), 7.63 (d, J = 7.2 Hz, 1H), 7.51–7.44 (m, 4H), 7.44–7.35 (m, 3H), 7.34-7.29 (m, 1H), 7.29-7.24 (m, 1H), 6.56 (s, 3.70H (fumarate)), 4.03 (s, 2H), 3.52 (s, 2H), 2.81 (app d, J = 11.4 Hz, 2H), 2.68 (br s, 2H), 2.04–1.96 (m, 2H), 1.72 (app d, J = 12.4 Hz, 2H), 1.61 (br s, 1H), 1.18 (qd, J = 12.1, 3.7 Hz, 2H). ^{13}C NMR (126 MHz, DMSO-d_6) δ 167.0, 140.3, 139.7, 135.8, 134.6, 134.3, 133.3, 130.8, 129.2, 129.1, 129.0, 128.8, 128.6, 128.2, 127.7, 127.0, 126.7, 126.6, 58.8, 52.7, 52.1, 50.8, 33.1, 29.6. HRMS-ESI m/z $[M + H]^+$ calc. for $C_{26}H_{31}ClN_2^+$ 405.2098; found 379.1937.

4.3.2.3.25. N-(3-chlorobenzyl)-1-(1-(2-chlorobenzyl)piperidin-4-yl)methanamine fumarate ***(27)***. The general procedure C was followed using **2** (0.155 g, 0.65 mmol), 3-chlorobenzaldehyde (0.091 g, 0.65 mmol), Na_2SO_4 (0.554 g, 3.90 mmol), DCM (12 mL) and a reaction time of 69 h. Imine reduction was performed with $NaBH_4$ (0.034 g, 0.91 mmol), MeOH (12 mL) and reaction time of 30 min, furnishing N-(3-chlorobenzyl)-1-(1-(2-chlorobenzyl)piperidin-4-yl)methanamine (0.185 g, 97% pure, 67% yield). Compound **27** was prepared as described for compound **21** using corresponding amine (0.067 g) in 2-PrOH (5 mL), a solution of fumaric acid (0.043 g, 0.60 mmol, theoretically 2.0 eq) in 2-PrOH (2 mL) and salt

formation time 2 h. Compound **27** was obtained as a white solid (0.062 g, overall yield 38%), containing 1.875 eq fumarate as a salt and is a 2-PrOH solvate (0.04 eq) as determined by NMR analysis. Mp: 212.4–220.1 °C. ^{1}H NMR (600 MHz, DMSO-d_6) δ 7.53 (s, 1H), 7.46 (d, J = 7.3 Hz, 1H), 7.44–7.34 (m, 4H), 7.32 (t, J = 7.2 Hz, 1H), 7.27 (t, J = 7.5 Hz, 1H), 6.57 (s, 3.75H (fumarate)), 3.93 (s, 2H), 3.53 (s, 2H), 2.81 (app d, J = 11.4 Hz, 2H), 2.60 (d, J = 6.7 Hz, 2H), 2.01 (app t, J = 11.9 Hz, 2H), 1.70 (app d, J = 14.4 Hz, 2H), 1.63–1.53 (m, 1H), 1.17 (qd, J = 12.3, 3.8 Hz, 2H). ^{13}C NMR (151 MHz, DMSO-d_6) δ 166.6, 138.7, 135.8, 134.4, 133.2, 133.0, 130.7, 130.2, 129.2, 128.8, 128.5, 127.7, 127.7, 127.0, 58.8, 52.0, 52.9, 50.9, 34.0, 29.8. HRMS-ESI m/z $[M + H]^+$ calc. for $C_{20}H_{25}Cl_2N_2^+$ 363.1395; found 363.1373.

Author contributions

IA and MG carried out the synthesis and analysis of compounds. SS, LR and MA conducted the computational studies. AZ, JPB, CPV and BC performed pharmacological characterization experiments. IA collected the data. IA, SS and AZ wrote the paper. RL, MW, IJPdE, HFV, SJB, SJH and CH reviewed the manuscript. RL, MW, IJPdE, HFV, CdG, MJS, SJB, CH, SJH supervised the project.

Conflicts of interest

The authors declare no potential conflicts of interest.

Acknowledgments

This work was supported by a European Union's Horizon 2020 MSCA Programme under grant agreement 641833 (ONCORNET to IA, MA, MJS, RL, CPV and CH), The Netherlands eScience Center (NLeSC)/NWO (Enabling Technologies project: 3D-e-Chem, grant 027.014.201 to CdG), NWO CW TOP-PUNT grant 718.014.002 (7 ways to 7TMR modulation, 7-to-7, to R.L. and M.J.S.) and China Scholarship Council (CSC grant to SS). SS, MA, MJS, RL, IJPdE, CH and CdG participate in the European Cooperation in Science and Technology Action CM1207 [GPCR–Ligand Interactions, Structures, and Transmembrane Signalling: A European Research Network (GLISTEN)] and the GPCR Consortium (gpcrconsortium.org). We thank Marlies C.A. Verkade-Vreeker, Hans Custers, Nailton M. Mascimento-Jr and Andrea van de Stolpe for technical assistance.

Appendix A. Supplementary data

Supplementary data to this article can be found online at https://doi.org/10.1016/j.ejmech.2018.10.060.

References

[1] D.J. Scholten, M. Canals, D. Maussang, L. Roumen, M.J. Smit, M. Wijtmans, C. de Graaf, H.F. Vischer, R. Leurs, Pharmacological modulation of chemokine receptor function, Br. J. Pharmacol. 165 (2012) 1617–1643.
[2] S.J. Allen, S.E. Crown, T.M. Handel, Chemokine: receptor structure, interactions, and antagonism, Annu. Rev. Immunol. 25 (2007) 787–820.
[3] G. Bongers, D. Maussang, L.R. Muniz, V.M. Noriega, A. Fraile-Ramos, N. Barker, F. Marchesi, N. Thirunarayanan, H.F. Vischer, L. Qin, L. Mayer, N. Harpaz, R. Leurs, G.C. Furtado, H. Clevers, D. Tortorella, M.J. Smit, S.A. Lira, The cytomegalovirus-encoded chemokine receptor US28 promotes intestinal neoplasia in transgenic mice, J. Clin. Invest. 120 (2010) 3969–3978.
[4] E. Slinger, D. Maussang, A. Schreiber, M. Siderius, A. Rahbar, A. Fraile-Ramos, S.A. Lira, C. Soderberg-Naucler, M.J. Smit, HCMV-encoded chemokine receptor US28 mediates proliferative signaling through the IL-6-STAT3 axis, Sci. Signal. 3 (2010) ra58.
[5] M. Arimont, S.L. Sun, R. Leurs, M. Smit, I.J.P. de Esch, C. de Graaf, Structural analysis of chemokine receptor-ligand interactions, J. Med. Chem. 60 (2017) 4735–4779.
[6] B. Wu, E.Y. Chien, C.D. Mol, G. Fenalti, W. Liu, V. Katritch, R. Abagyan, A. Brooun, P. Wells, F.C. Bi, D.J. Hamel, P. Kuhn, T.M. Handel, V. Cherezov, R.C. Stevens, Structures of the CXCR4 chemokine GPCR with small-molecule and cyclic peptide antagonists, Science 330 (2010) 1066–1071.
[7] L. Qin, I. Kufareva, L.G. Holden, C. Wang, Y. Zheng, C. Zhao, G. Fenalti, H. Wu, G.W. Han, V. Cherezov, R. Abagyan, R.C. Stevens, T.M. Handel, Structural biology. Crystal structure of the chemokine receptor CXCR4 in complex with a viral chemokine, Science 347 (2015) 1117–1122.
[8] Y. Zheng, G.W. Han, R. Abagyan, B. Wu, R.C. Stevens, V. Cherezov, I. Kufareva, T.M. Handel, Structure of CC chemokine receptor 5 with a potent chemokine antagonist reveals mechanisms of chemokine recognition and molecular mimicry by HIV, Immunity 46 (2017) 1005–1017, e1005.
[9] J.S. Burg, J.R. Ingram, A.J. Venkatakrishnan, K.M. Jude, A. Dukkipati, E.N. Feinberg, A. Angelini, D. Waghray, R.O. Dror, H.L. Ploegh, K.C. Garcia, Structural biology. Structural basis for chemokine recognition and activation of a viral G protein-coupled receptor, Science 347 (2015) 1113–1117.
[10] M. Congreve, C. Oswald, F.H. Marshall, Applying structure-based drug design approaches to allosteric modulators of GPCRs, Trends Pharmacol. Sci. 38 (2017) 837–847.
[11] Q. Tan, Y. Zhu, J. Li, Z. Chen, G.W. Han, I. Kufareva, T. Li, L. Ma, G. Fenalti, J. Li, W. Zhang, X. Xie, H. Yang, H. Jiang, V. Cherezov, H. Liu, R.C. Stevens, Q. Zhao, B. Wu, Structure of the CCR5 chemokine receptor-HIV entry inhibitor maraviroc complex, Science 341 (2013) 1387–1390.
[12] Y. Zheng, L. Qin, N.V. Zacarias, H. de Vries, G.W. Han, M. Gustavsson, M. Dabros, C. Zhao, R.J. Cherney, P. Carter, D. Stamos, R. Abagyan, V. Cherezov, R.C. Stevens, I.J. AP, L.H. Heitman, A. Tebben, I. Kufareva, T.M. Handel, Structure of CC chemokine receptor 2 with orthosteric and allosteric antagonists, Nature 540 (2016) 458–461.
[13] C. Oswald, M. Rappas, J. Kean, A.S. Dore, J.C. Errey, K. Bennett, F. Deflorian, J.A. Christopher, A. Jazayeri, J.S. Mason, M. Congreve, R.M. Cooke, F.H. Marshall, Intracellular allosteric antagonism of the CCR9 receptor, Nature 540 (2016) 462–465.
[14] N.V. Ortiz Zacarias, E.B. Lenselink, I.J. AP, T.M. Handel, L.H. Heitman, Intracellular receptor modulation: novel approach to target GPCRs, Trends Pharmacol. Sci. 39 (2018) 547–559.
[15] M. Chaturvedi, J. Schilling, A. Beautrait, M. Bouvier, J.L. Benovic, A.K. Shukla, Emerging paradigm of intracellular targeting of G protein-coupled receptors, Trends Biochem. Sci. 43 (2018) 533–546.
[16] A.J. Kooistra, S. Kuhne, I.J. de Esch, R. Leurs, C. de Graaf, A structural chemogenomics analysis of aminergic GPCRs: lessons for histamine receptor ligand design, Br. J. Pharmacol. 170 (2013) 101–126.
[17] E.P. Istyastono, A.J. Kooistra, H.F. Vischer, M. Kuijer, L. Roumen, S. Nijmeijer, R.A. Smits, I.J.P. de Esch, R. Leurs, C. de Graaf, Structure-based virtual screening for fragment-like ligands of the G protein-coupled histamine H4 receptor, MedChemComm 6 (2015) 1003–1017.
[18] S. Hatse, K. Princen, G. Bridger, E. De Clercq, D. Schols, Chemokine receptor inhibition by AMD3100 is strictly confined to CXCR4, FEBS Lett. 527 (2002) 255–262.
[19] Z.G. Zachariassen, S. Karlshoj, B.E. Haug, M.M. Rosenkilde, J. Vabeno, Probing the molecular interactions between CXC chemokine receptor 4 (CXCR4) and an arginine-based tripeptidomimetic antagonist (KRH-1636), J. Med. Chem. 58 (2015) 8141–8153.
[20] Z. Chongqian, H. Tingjun, F. Zhiwei, L. Youyong, Structure-based development of antagonists for chemokine receptor CXCR4, Curr. Comput. Aided Drug Des. 9 (2013) 60–75.
[21] I. Kufareva, M. Rueda, V. Katritch, R.C. Stevens, R. Abagyan, G.D. participants, Status of GPCR modeling and docking as reflected by community-wide GPCR Dock 2010 assessment, Structure 19 (2011) 1108–1126.
[22] G. Thoma, M.B. Streiff, J. Kovarik, F. Glickman, T. Wagner, C. Beerli, H.-G. Zerwes, Orally bioavailable isothioureas block function of the chemokine receptor CXCR4 in vitro and in vivo, J. Med. Chem. 51 (2008) 7915–7920.
[23] W.B. Zhang, J.M. Navenot, B. Haribabu, H. Tamamura, K. Hiramatu, A. Omagari, G. Pei, J.P. Manfredi, N. Fujii, J.R. Broach, S.C. Peiper, A point mutation that confers constitutive activity to CXCR4 reveals that T140 is an inverse agonist and that AMD3100 and ALX40-4C are weak partial agonists, J. Biol. Chem. 277 (2002) 24515–24521.
[24] W. Zhan, Z. Liang, A. Zhu, S. Kurtkaya, H. Shim, J.P. Snyder, D.C. Liotta, Discovery of small molecule CXCR4 antagonists, J. Med. Chem. 50 (2007) 5655–5664.
[25] E. Inokuchi, S. Oishi, T. Kubo, H. Ohno, K. Shimura, M. Matsuoka, N. Fujii, Potent CXCR4 antagonists containing amidine type Peptide bond isosteres, ACS Med. Chem. Lett. 2 (2011) 477–480.
[26] W.T. Choi, S. Duggineni, Y. Xu, Z. Huang, J. An, Drug discovery research targeting the CXC chemokine receptor 4 (CXCR4), J. Med. Chem. 55 (2012) 977–994.
[27] F. Grande, G. Giancotti, G. Ioele, M.A. Occhiuzzi, A. Garofalo, An update on small molecules targeting CXCR4 as starting points for the development of anti-cancer therapeutics, Eur. J. Med. Chem. 139 (2017) 519–530.
[28] E.J. Miller, E. Jecs, V.M. Truax, B.M. Katzman, Y.A. Tahirovic, R.J. Wilson, K.M. Kuo, M.B. Kim, H.H. Nguyen, M.T. Saindane, H. Zhao, T. Wang, C.S. Sum, M.E. Cvijic, G.M. Schroeder, L.J. Wilson, D.C. Liotta, Discovery of tetrahydroisoquinoline-containing CXCR4 antagonists with improved in vitro ADMET properties, J. Med. Chem. 61 (2018) 946–979.
[29] Y.A. Tahirovic, V.M. Truax, R.J. Wilson, E. Jecs, H.H. Nguyen, E.J. Miller, M.B. Kim, K.M. Kuo, T. Wang, C.S. Sum, M.E. Cvijic, G.M. Schroeder, L.J. Wilson, D.C. Liotta, Discovery of N-alkyl piperazine side chain based CXCR4 antagonists with improved drug-like properties, ACS Med. Chem. Lett. 9 (2018) 446–451.
[30] D. Das, K. Maeda, Y. Hayashi, N. Gavande, D.V. Desai, S.B. Chang, A.K. Ghosh, H. Mitsuya, Insights into the mechanism of inhibition of CXCR4: identification of Piperidinylethanamine analogs as anti-HIV-1 inhibitors, Antimicrob. Agents Chemother. 59 (2015) 1895–1904.

[31] M.M. Mysinger, D.R. Weiss, J.J. Ziarek, S. Gravel, A.K. Doak, J. Karpiak, N. Heveker, B.K. Shoichet, B.F. Volkman, Structure-based ligand discovery for the protein-protein interface of chemokine receptor CXCR4, Proc. Natl. Acad. Sci. U. S. A. 109 (2012) 5517–5522.

[32] Y. Wang, W.-C. Liang, W.-L. Pan, W.-K. Law, J.-S. Hu, D.T.-M. Ip, M.M.-Y. Waye, T.-B. Ng, D.C.-C. Wan, Silibinin, a novel chemokine receptor type 4 antagonist, inhibits chemokine ligand 12-induced migration in breast cancer cells, Phytomedicine 21 (2014) 1310–1317.

[33] J. Kim, M.L. Yip, X. Shen, H. Li, L.Y. Hsin, S. Labarge, E.L. Heinrich, W. Lee, J. Lu, N. Vaidehi, Identification of anti-malarial compounds as novel antagonists to chemokine receptor CXCR4 in pancreatic cancer cells, PLoS One 7 (2012), e31004.

[34] A.L. Hopkins, C.R. Groom, A. Alex, Ligand efficiency: a useful metric for lead selection, Drug Discov. Today 9 (2004) 430–431.

[35] G.E. de Kloe, D. Bailey, R. Leurs, I.J. de Esch, Transforming fragments into candidates: small becomes big in medicinal chemistry, Drug Discov. Today 14 (2009) 630–646.

[36] D. Rognan, Fragment-based approaches and computer-aided drug discovery, Top. Curr. Chem. 317 (2012) 201–222.

[37] L. Ros-Blanco, J. Anido, R. Bosser, J. Este, B. Clotet, A. Kosoy, L. Ruiz-Avila, J. Teixido, J. Seoane, J.I. Borrell, Noncyclam tetraamines inhibit CXC chemokine receptor type 4 and target glioma-initiating cells, J. Med. Chem. 55 (2012) 7560–7570.

[38] B.D. Cox, A.R. Prosser, Y. Sun, Z. Li, S. Lee, M.B. Huang, V.C. Bond, J.P. Snyder, M. Krystal, L.J. Wilson, D.C. Liotta, Pyrazolo-piperidines exhibit dual inhibition of CCR5/CXCR4 HIV entry and reverse transcriptase, ACS Med. Chem. Lett. 6 (2015) 753–757.

[39] S.R. Mooring, J. Liu, Z. Liang, J. Ahn, S. Hong, Y. Yoon, J.P. Snyder, H. Shim, Benzenesulfonamides: a unique class of chemokine receptor type 4 inhibitors, ChemMedChem 8 (2013) 622–632.

[40] J.F. Miller, E.M. Turner, K.S. Gudmundsson, S. Jenkinson, A. Spaltenstein, M. Thomson, P. Wheelan, Novel N-substituted benzimidazole CXCR4 antagonists as potential anti-HIV agents, Bioorg. Med. Chem. Lett 20 (2010) 2125–2128.

[41] C. de Graaf, H.F. Vischer, G.E. de Kloe, A.J. Kooistra, S. Nijmeijer, M. Kuijer, M.H. Verheij, P.J. England, J.E. van Muijlwijk-Koezen, R. Leurs, I.J. de Esch, Small and colorful stones make beautiful mosaics: fragment-based chemogenomics, Drug Discov. Today 18 (2013) 323–330.

[42] G. Jones, P. Willett, R.C. Glen, A.R. Leach, R. Taylor, Development and validation of a genetic algorithm for flexible docking, J. Mol. Biol. 267 (1997) 727–748.

[43] O. Korb, T. Stützle, T. Exner, An ant colony optimization approach to flexible protein–ligand docking, Swarm. Intell. 1 (2007) 115–134.

[44] G. Marcou, D. Rognan, Optimizing fragment and scaffold docking by use of molecular interaction fingerprints, J. Chem. Inf. Model. 47 (2007) 195–207.

[45] J.S. Mason, A. Bortolato, M. Congreve, F.H. Marshall, New insights from structural biology into the druggability of G protein-coupled receptors, Trends Pharmacol. Sci. 33 (2012) 249–260.

[46] M. Wawer, J. Bajorath, Similarity-potency trees: a method to search for SAR information in compound data sets and derive SAR rules, J. Chem. Inf. Model. 50 (2010) 1395–1409.

[47] M. Vass, A.J. Kooistra, T. Ritschel, R. Leurs, I.J. de Esch, C. de Graaf, Molecular interaction fingerprint approaches for GPCR drug discovery, Curr. Opin. Pharmacol. 30 (2016) 59–68.

[48] S. Schultes, C. de Graaf, E.E.J. Haaksma, I.J.P. de Esch, R. Leurs, O. Krämer, Ligand efficiency as a guide in fragment hit selection and optimization, Drug Discov. Today Technol. 7 (2010) e157–e162.

[49] E.P. Istyastono, S. Nijmeijer, H.D. Lim, A. van de Stolpe, L. Roumen, A.J. Kooistra, H.F. Vischer, I.J. de Esch, R. Leurs, C. de Graaf, Molecular determinants of ligand binding modes in the histamine H(4) receptor: linking ligand-based three-dimensional quantitative structure-activity relationship (3D-QSAR) models to in silico guided receptor mutagenesis studies, J. Med. Chem. 54 (2011) 8136–8147.

[50] S. Malhotra, J. Karanicolas, When does chemical elaboration induce a ligand to change its binding mode? J. Med. Chem. 60 (2017) 128–145.

[51] P.D. Leeson, B. Springthorpe, The influence of drug-like concepts on decision-making in medicinal chemistry, Nat. Rev. Drug Discov. 6 (2007) 881–890.

[52] S. Jahnichen, C. Blanchetot, D. Maussang, M. Gonzalez-Pajuelo, K.Y. Chow, L. Bosch, S. De Vrieze, B. Serruys, H. Ulrichts, W. Vandevelde, M. Saunders, H.J. De Haard, D. Schols, R. Leurs, P. Vanlandschoot, T. Verrips, M.J. Smit, CXCR4 nanobodies (VHH-based single variable domains) potently inhibit chemotaxis and HIV-1 replication and mobilize stem cells, Proc. Natl. Acad. Sci. U. S. A. 107 (2010) 20565–20570.

[53] C. Dezi, A. Carotti, M. Magnani, M. Baroni, A. Padova, G. Cruciani, A. Macchiarulo, R. Pellicciari, Molecular interaction fields and 3D-QSAR studies of p53-MDM2 inhibitors suggest additional features of ligand-target interaction, J. Chem. Inf. Model. 50 (2010) 1451–1465.

[54] P.J. Goodford, A computational procedure for determining energetically favorable binding sites on biologically important macromolecules, J. Med. Chem. 28 (1985) 849–857.

[55] J.A. Ballesteros, H. Weinstein, Integrated methods for the construction of three-dimensional models and computational probing of structure-function relations in G protein-coupled receptors, Methods Neurosci. 25 (1995) 366–428.

[56] J.J. Irwin, B.K. Shoichet, ZINC–a free database of commercially available compounds for virtual screening, J. Chem. Inf. Model. 45 (2005) 177–182.

[57] M.H. Verheij, C. de Graaf, G.E. de Kloe, S. Nijmeijer, H.F. Vischer, R.A. Smits, O.P. Zuiderveld, S. Hulscher, L. Silvestri, A.J. Thompson, J.E. van Muijlwijk-Koezen, S.C. Lummis, R. Leurs, I.J. de Esch, Fragment library screening reveals remarkable similarities between the G protein-coupled receptor histamine H(4) and the ion channel serotonin 5-HT(3)A, Bioorg. Med. Chem. Lett 21 (2011) 5460–5464.

[58] G. Siegal, E. Ab, J. Schultz, Integration of fragment screening and library design, Drug Discov. Today 12 (2007) 1032–1039.

[59] FILTER, Version 2.1.1; OpenEye Scientific Software: Santa Fe, NM.

[60] Calculator, Version 5.1.4; ChemAxon: Budapest, Hungary.

[61] Corina, Version 3.46; Molecular Networks GmbH: Erlangen, Germany.

[62] MOE, Version 2010.10; Chemical Computing Group, Inc.: Montreal, Canada.

[63] O. Korb, T. Stutzle, T.E. Exner, Empirical scoring functions for advanced protein-ligand docking with PLANTS, J. Chem. Inf. Model. 49 (2009) 84–96.

[64] C. de Graaf, D. Rognan, Selective structure-based virtual screening for full and partial agonists of the beta2 adrenergic receptor, J. Med. Chem. 51 (2008) 4978–4985.

[65] C. de Graaf, A.J. Kooistra, H.F. Vischer, V. Katritch, M. Kuijer, M. Shiroishi, S. Iwata, T. Shimamura, R.C. Stevens, I.J. de Esch, R. Leurs, Crystal structure-based virtual screening for fragment-like ligands of the human histamine H(1) receptor, J. Med. Chem. 54 (2011) 8195–8206.

[66] D. Rogers, M. Hahn, Extended-connectivity fingerprints, J. Chem. Inf. Model. 50 (2010) 742–754.

[67] M.P. Mazanetz, R.J. Marmon, C.B. Reisser, I. Morao, Drug discovery applications for KNIME: an open source data mining platform, Curr. Top. Med. Chem. 12 (2012) 1965–1979.

[68] H.J.C. Berendsen, D. van der Spoel, R. van Drunen, GROMACS: a message-passing parallel molecular dynamics implementation, Comput. Phys. Commun. 91 (1995) 43–56.

[69] A. Cordomi, G. Caltabiano, L. Pardo, Membrane protein simulations using AMBER Force field and berger lipid parameters, J. Chem. Theor. Comput. 8 (2012) 948–958.

[70] A. Jakalian, D.B. Jack, C.I. Bayly, Fast, efficient generation of high-quality atomic charges. AM1-BCC model: II. Parameterization and validation, J. Comput. Chem. 23 (2002) 1623–1641.

[71] MOE, Version 2013.0801; Chemical Computing Group, Inc.: Montreal, Canada.

[72] M. Pastor, G. Cruciani, K.A. Watson, A strategy for the incorporation of water molecules present in a ligand binding site into a three-dimensional quantitative structure–activity relationship analysis, J. Med. Chem. 40 (1997) 4089–4102.

[73] R: a Language and Environment for Statistical Computing, R Development Core Team, Vienna, Austria, 2008. http://www.Rproject.org.

[74] Eibe Frank, Mark A. Hall, Ian H. Witten, The WEKA Workbench. Online Appendix for "Data Mining: Practical Machine Learning Tools and Techniques", fourth ed., Morgan Kaufmann, 2016.

[75] D. Verzijl, S. Storelli, D.J. Scholten, L. Bosch, T.A. Reinhart, D.N. Streblow, C.P. Tensen, C.P. Fitzsimons, G.J. Zaman, J.E. Pease, I.J. de Esch, M.J. Smit, R. Leurs, Noncompetitive antagonism and inverse agonism as mechanism of action of nonpeptidergic antagonists at primate and rodent CXCR3 chemokine receptors, J. Pharmacol. Exp. Therapeut. 325 (2008) 544–555.

[76] H.F. Vischer, S. Nijmeijer, M.J. Smit, R. Leurs, Viral hijacking of human receptors through heterodimerization, Biochem. Biophys. Res. Commun. 377 (2008) 93–97.

[77] S. Nijmeijer, H. Engelhardt, S. Schultes, A.C. van de Stolpe, V. Lusink, C. de Graaf, M. Wijtmans, E.E. Haaksma, I.J. de Esch, K. Stachurski, H.F. Vischer, R. Leurs, Design and pharmacological characterization of VUF14480, a covalent partial agonist that interacts with cysteine 98(3.36) of the human histamine H(4) receptor, Br. J. Pharmacol. 170 (2013) 89–100.

[78] J. van Unen, A.D. Stumpf, B. Schmid, N.R. Reinhard, P.L. Hordijk, C. Hoffmann, T.W. Gadella Jr., J. Goedhart, A new generation of FRET sensors for robust measurement of Galphai1, Galphai2 and Galphai3 activation kinetics in single cells, PLoS One 11 (2016), e0146789.

[79] L.A. Stoddart, E.K.M. Johnstone, A.J. Wheal, J. Goulding, M.B. Robers, T. Machleidt, K.V. Wood, S.J. Hill, K.D.G. Pfleger, Application of BRET to monitor ligand binding to GPCRs, Nat. Methods 12 (2015) 661–663.

[80] L.A. Stoddart, A.J. Vernall, M. Bouzo-Lorenzo, R. Bosma, A.J. Kooistra, C. de Graaf, H.F. Vischer, R. Leurs, S.J. Briddon, B. Kellam, S.J. Hill, Development of novel fluorescent histamine H1-receptor antagonists to study ligand-binding kinetics in living cells, Sci. Rep. 8 (2018) 1572.